



THE UNIVERSITY *of* EDINBURGH

## Edinburgh Research Explorer

# Impact of recycling and lateral sediment input on grain size fining trends – implications for reconstructing tectonic and climate forcings in ancient sedimentary systems

### Citation for published version:

Harries, R, Kirstein, L, Whittaker, A, Attal, M & Main, I 2019, 'Impact of recycling and lateral sediment input on grain size fining trends – implications for reconstructing tectonic and climate forcings in ancient sedimentary systems', *Basin Research*. <https://doi.org/10.1111/bre.12349>

### Digital Object Identifier (DOI):

[10.1111/bre.12349](https://doi.org/10.1111/bre.12349)

### Link:

[Link to publication record in Edinburgh Research Explorer](#)

### Document Version:

Peer reviewed version

### Published In:

Basin Research

### General rights

Copyright for the publications made accessible via the Edinburgh Research Explorer is retained by the author(s) and / or other copyright owners and it is a condition of accessing these publications that users recognise and abide by the legal requirements associated with these rights.

### Take down policy

The University of Edinburgh has made every reasonable effort to ensure that Edinburgh Research Explorer content complies with UK legislation. If you believe that the public display of this file breaches copyright please contact [openaccess@ed.ac.uk](mailto:openaccess@ed.ac.uk) providing details, and we will remove access to the work immediately and investigate your claim.



# Impact of recycling and lateral sediment input on grain size fining trends – implications for reconstructing tectonic and climate forcings in ancient sedimentary systems

**Rebekah Harries**\*<sup>1</sup>, L. A. Kirstein<sup>1</sup>, A. Whittaker<sup>2</sup>, M. Attal<sup>1</sup>, Ian Main<sup>1</sup>

<sup>1</sup>The University of Edinburgh, <sup>2</sup>Imperial College London

\*Corresponding author email: [rebekah.m.harries@gmail.com](mailto:rebekah.m.harries@gmail.com)

## 1 Abstract

2

3 Grain size trends in basin stratigraphy are thought to preserve a rich record of the climatic and tectonic  
4 controls on landscape evolution. Stratigraphic models assume that over geological timescales, the  
5 downstream profile of sediment deposition is in dynamic equilibrium with the spatial distribution of  
6 tectonic subsidence in the basin, sea level and the flux and calibre of sediment supplied from mountain  
7 catchments. Here we demonstrate that this approach to modelling stratigraphic responses to  
8 environmental change is missing a key ingredient: the dynamic geomorphology of the sediment  
9 routing system. For three large alluvial fans in the Iglesia basin, Argentine Andes we measured the  
10 grain size of modern river sediment from fan apex to toe and characterise the spatial distribution of  
11 differential subsidence for each fan by constructing a 3D model of basin stratigraphy from seismic  
12 data. We find, using a self-similar grain size fining model, that the profile of grain size fining on all  
13 three fans cannot be reproduced given the subsidence profile measured and for any sediment supply  
14 scenario. However, by adapting the self-similar model, we demonstrate that the grain size trends on  
15 each fan can be effectively reproduced when sediment is not only sourced from a single catchment at  
16 the apex of the system, but also laterally, from tributary catchments and through fan surface recycling.  
17 Without constraint on the dynamic geomorphology of these large alluvial systems, signals of tectonic  
18 and climate forcing in grain size data are masked and would be indecipherable in the geological record.  
19 This has significant implications for our ability to make sensitive, quantitative reconstructions of  
20 external boundary conditions from the sedimentary record.

## 21 1. Introduction

### 22 1.1. Rationale

23  
24 The grain size and rate of fining downstream of alluvial sediment are key physical attributes that can  
25 store important environmental information (Heller & Paola, 1992; Robinson & Slingerland, 1998; Hoey  
26 & Bluck, 1999; Duller *et al.*, 2010). Climatic and tectonic boundary conditions are documented to  
27 control the volume and calibre of sediment released into depositional basins (Hovius & Leeder, 1998;  
28 Allen *et al.*, 2017; Roda-Boluda & Whittaker, 2018). This sediment is then deposited downstream at a  
29 rate controlled both by the spatial distribution of tectonic subsidence and the dynamics of sediment  
30 transport and deposition (Fedele & Paola, 2007; Duller *et al.*, 2010; Whittaker *et al.*, 2011).  
31 Quantitative inversions of downstream grain size trends for the rate of sediment supply and  
32 accommodation generation could therefore provide a window into the climatic and tectonic settings  
33 of the past (e.g. Duller *et al.*, 2010; Allen *et al.*, 2013) with recent studies linking changing grain size  
34 fining rate in alluvial fan settings to both tectonic and environmental drivers (e.g. Parsons *et al.*, 2012;  
35 D'Arcy *et al.*, 2017). However, numerical models and flume experiments have shown that dynamic  
36 fluctuations in bed surface morphology over geomorphic timescales can buffer the transfer of an  
37 environmental signal into depositional stratigraphy (Humphrey & Heller, 1995; Jerolmack & Paola,  
38 2010), even where input sediment fluxes from upland catchments can be linked to changing climate  
39 (Waters *et al.*, 2010; McPhillips *et al.*, 2013; D'Arcy *et al.*, 2017). Moreover, while numerical models of  
40 sediment routing systems are capable of producing convincing stratigraphic patterns (Allen &  
41 Densmore, 2000; Armitage *et al.*, 2011; Allen & Heller, 2012; Forzoni *et al.*, 2014), they often fail to  
42 consider how sediment recycling and multiple sediment inputs influence the mass balance of the  
43 system and the distribution of grain sizes in a basin over geologically meaningful timescales (Rice,  
44 1998; Malatesta *et al.*, 2017; Malatesta *et al.*, 2018). A better understanding of this problem is crucial  
45 to characterise the sensitivity of the fluvial systems at the Earth's surface to changing tectono-climatic  
46 boundary conditions over a range of spatial and temporal scales (Pelletier *et al.*, 2015; Romans *et al.*,  
47 2016).

48 For fluvial systems transporting abrasion-resistant clasts as bedload, classical models solving the  
49 downstream distribution of grain sizes on a river bed emulate the hydraulically driven, size selectivity  
50 of sediment transport processes that are well-documented in laboratory flume experiments (e.g.  
51 Parker, 1991a; Paola & Seal, 1995; Hoey & Ferguson, 1997). For instance, a poorly sorted sediment  
52 load, fed to the apex of the flume, will fractionate downstream due to the preferential deposition of  
53 coarser clasts, at a rate controlled by the rivers transport capacity and its sediment supply (Paola *et*  
54 *al.*, 1992; Seal *et al.*, 1997). However, in natural systems, tributaries, hillslopes and the recycling of  
55 fluvial terraces introduce significant additional sources of sediment laterally into the system, so that  
56 the downstream fractionation of grain sizes integrates both local and downstream sediment supplies  
57 (Pizzuto, 1995; Rice, 1998; Rice & Church, 1998; Rice, 1999). The processing of lateral inputs of  
58 sediment has been highlighted as a potential buffer for the translation of environmental signals into  
59 stratigraphy and is a major source of uncertainty in numerical models of sediment routing systems  
60 (Rice & Church, 1998; Jerolmack & Paola, 2010; Allen *et al.*, 2017; Malatesta *et al.*, 2017). To-date a  
61 number of field observations report lateral sediment inputs having variable impacts on downstream  
62 fining trends (Church & Kellerhals, 1978; Constantine *et al.*, 2003). There is evidence in some rivers for  
63 lateral inputs redefining the particle size distribution along the main river channel (Rice, 1998; Rice &  
64 Church, 1998; Constantine *et al.*, 2003; Attal & Lavé, 2006; Whittaker *et al.*, 2010; Attal *et al.*, 2015).  
65 Rice (1999) developed the term 'sedimentary links' to describe longitudinal sections of river, between  
66 tributary confluences, which have distinctly different rates of downstream fining. In other cases, a  
67 consistent rate of downstream fining is preserved along the river and there is little evidence of lateral  
68 sediment inputs having any persistent impact on surface size distributions (Hoey & Bluck, 1999; Gomez  
69 *et al.*, 2001; Singer, 2008). Ferguson *et al.* (2006) demonstrate that the interplay between water  
70 discharge, sediment flux and sediment size at tributary confluences impact the river's long profile and  
71 local grain size variability. Whether lateral inputs disrupt, perturb or have no influence on grain size  
72 fining trends has been tied to disparity between the relative volumes and grain sizes of the mixing  
73 loads and is likely a function of the degree of sorting of the lateral input supply during transport

74 between sediment source region and confluence (Singer, 2008). In this paper, we evaluate the impact  
75 lateral inputs of sediment have on grain size fining in Holocene streamflow-dominated gravel deposits  
76 by using alluvial fans in the Iglesia basin as a case study to assess the impact of multiple sediment  
77 inputs in modulating grain size fining where basin subsidence rates and source catchment sediment  
78 fluxes can be constrained independently. We use this data to evaluate the circumstances in which  
79 sediment recycling impedes the extraction of tectono-climatic signals from grain size fining trends  
80 from Holocene depositional systems.

## 81 1.2. Approach

82  
83 Probabilistic modelling of down-system grain size fining patterns as sediment is supplied laterally and  
84 moved axially requires knowledge of a large number of hydraulic variables to constrain the grain scale  
85 processes controlling bedload mixing and deposition along a channel reach (Parker, 1991b; Paola &  
86 Seal, 1995; Hoey & Ferguson, 1997; Robinson & Slingerland, 1998; Wilcock & Kenworthy, 2002). In  
87 making several simplifying assumptions, Ferguson et al. (2006) applied a 1D numerical model to  
88 investigate the impact of a tributary on the width-averaged bed elevation and grain size distribution  
89 along a channel profile. This approach recognised the complex evolution of sediment flux, water  
90 discharge and bedload diameter ratios between the mainstream and a tributary and their impact on  
91 channel aggradation or degradation and grain size along the river. However, it is also recognised that  
92 the rate of downstream grain size fining often scales, to a first order, with the size of the depositional  
93 system (Hoey & Bluck, 1999), indicating that transient fluctuations in a river's bed surface have limited  
94 impact on their grain size profiles. Fedele and Paola (2007) offered a deterministic solution for  
95 downstream grain size fining that simplifies the complexities of sediment transport over large  
96 temporal and spatial scales. Their solution is based on observations from numerical models and flume  
97 experiments that find aggrading rivers that reach near steady state develop self-similar substrate size  
98 distributions along substrate fining profiles that are positively correlated with self-similar bed profiles.

99 Fedele and Paola (2007) tie this self-organising behaviour to the well documented mechanism by  
 100 which channels modify their morphology in order to maintain a dimensionless shear stress slightly  
 101 above the critical Shields stress required for incipient motion (Shields, 1936; Parker, 1978; Buffington  
 102 & Montgomery, 1997; Mueller *et al.*, 2005; Lamb *et al.*, 2008). A constant value of the critical Shields  
 103 stress is often used to scale bedload sediment transport in numerical models (e.g. Meyer-Peter &  
 104 Muller, 1948). By invoking a constant Shields stress, specific to a bedload regime for gravel transport,  
 105 Fedele and Paola (2007) are able to characterise the relative mobility of clast sizes from an inversion  
 106 of the self-similar size distribution of clasts on the bed surface. They define their relative mobility  
 107 function as  $J_i = p_i/F_i$  where  $p_i$  represents the proportion of the  $i$ th grain size fraction in transport  
 108 and  $F_i$  is the proportion of that fraction in the bed surface(c.f. Paola & Seal, 1995). More detail on  $J_i$   
 109 is provided in the appendix. The partitioning of variance in the sediment supply between local  
 110 variability at a sample site and the variance in the downstream direction, which manifests as  
 111 downstream fining, can therefore be solved analytically using  $J_i$  and the wider mass balance of the  
 112 sediment routing system.

113 The starting point for Fedele and Paola's (2007) solution for downstream grain size fining describes  
 114 sediment deposition using a fractional Exner sediment mass balance:

$$115 \quad (1 - \lambda_p) \left( r_{\delta t}(X) + \frac{\delta \eta}{\delta t}(X) \right) = - \frac{\delta q_s}{\delta X} \quad \text{Equation 1}$$

116 where the rate of change in sediment discharge with downstream distance,  $\delta q_s / \delta X$ , is a function of  
 117 the longitudinal spatial distribution of tectonic subsidence over time,  $r_{\delta t}(X)$ , the rate of change in  
 118 bed elevation at a given downstream distance,  $\delta \eta / \delta t(X)$ , and sediment porosity,  $\lambda_p$ . This equation  
 119 can be rearranged to construct a 2D horizontal profile of mass extraction from an initial sediment flux,  
 120  $q_{s0}$ , along the total length,  $L$ , of a depositional system:

$$121 \quad q_s(X) = q_{s0} - (1 - \lambda_p) \int_0^L r_{\delta t}(X) dX \quad \text{Equation 2}$$

122 Fedele and Paola (2007) show that the fraction of a given sediment size deposited,  $f$ , from a  
123 transported load at any dimensionless downstream distance  $x^*$ , where  $x^* = X/L$ , can be solved for  
124 any distribution of mass deposited down-system,  $R^*$  :

$$125 \quad R^*(x^*) = (1 - \lambda_p)L \frac{r^*(x^*)}{q_s(x^*)} \quad \text{Equation 3}$$

126 Assuming geomorphic fluctuations in the bed surface are transient over long timescales,  $R^*$  is a ratio  
127 of the space made available for deposition by tectonic subsidence,  $r^*(x^*)$ , and the flux of sediment  
128 supplied to fill the space,  $q_s(x^*)$ . In such cases, the distribution of sediment extraction is described by  
129 a simple mass conserving sorting process and can be solved:

$$130 \quad \frac{df}{dx^*} = f \left[ R^* \left( 1 - \frac{1}{J_i} \right) - \frac{1}{J_i} \frac{dJ_i}{dx^*} \right] \quad \text{Equation 4}$$

131 Although not specifically addressed by Fedele and Paola (2007) and subsequent authors (e.g. Duller *et*  
132 *al.*, 2010), this approach sets up a mass balance framework that would in principle allow us to treat  
133 the mixing of lateral inputs with trunk stream inputs as function of their relative fluxes and grain size  
134 distributions. We are able to vary  $q_s(x^*)$  as a discontinuous function of  $x^*$ . It is therefore a powerful  
135 tool that can be used to better understand how lateral inputs of sediment might impact the  
136 downstream fining of grain sizes in a sediment routing system over stratigraphic timescales.

137 In this paper, we apply Fedele and Paola's (2007) 2D self-similar solution for downstream grain size  
138 fining to field data collected from three large, arid alluvial fans in the Iglesia basin, south central  
139 Argentine Andes. We exploit the Fedele and Paola (2007) model to examine the impact of sediment  
140 recycling and tributaries on downstream grain size fining trends on alluvial fans. In particular we adapt  
141 the mass balance framework within the model to account for lateral inputs from both tributary and  
142 recycled terrace sources.



## 143 2. Study Area

144 The Iglesia basin is a wedge-top, piggyback basin, separating the Frontal Cordillera of the Argentine  
145 Andes on the west, from a thin-skinned, Precordillera fold and thrust belt to the east (Allmendinger *et*  
146 *al.*, 1990; Suriano *et al.*, 2015) (figure 1). These structures accommodated compression from the  
147 shallow subduction of the Nazca plate throughout the Neogene and translated the Iglesia basin  
148 passively on top of the westernmost thrust sheet (Alvarez-Marron *et al.*, 2006). The tectonic, climatic  
149 and base level controls on the evolution of the Iglesia basin have received much attention due to the  
150 large amount of data available on the basin's stratigraphy. We use these data, outlined below, to  
151 constrain the distribution of accommodation within the basin at high resolution.

152 A 48-channel active-source reflection seismic survey, sampling the majority of the basin's longitudinal  
153 axis, was carried out in 1980-1981 by Argentine oil company Yacimientos Petroliferos Fiscales. These  
154 data have been analysed by several authors (Snyder, 1988; Beer *et al.*, 1990; Fernández-Seveso, 1993;  
155 Ruskin & Jordan, 2007). The shape of the basin is controlled by tectonic movement on the basins  
156 margins as well as on intrabasinal thrusts associated with the El Tigre strike-slip deformation zone  
157 (Allmendinger *et al.*, 1990). In the centre of the basin, the fill is ~3.5 km thick. To the west, strata  
158 decrease in thickness and onlap onto a basement surface that dips 12° east (Allmendinger *et al.*, 1990;  
159 Ruskin & Jordan, 2007). Allmendinger *et al.* (1990) observe that although there is a change in slope  
160 between the Frontal Cordillera and the basin, there is no surface-breaking thrust, suggesting the  
161 Frontal Cordillera uplifted as a growing fault-bend anticline over a buried ramp, effectively tilting the  
162 basin to the east. In the east of the basin, fault-propagation folds associated with intrabasinal thrusts  
163 at depth, have exposed the entirety of the basin fill in surface outcrops (Ruskin & Jordan, 2007).  
164 Alvarez-Marron *et al.* (2006) interprets the large-scale architecture of these out-of-sequence thrusts  
165 as a positive flower structure, where Miocene and Pliocene sedimentation was synchronous with  
166 faulting. Ruskin and Jordan (2007) identify eleven sequence boundaries within the basin's fill, as  
167 shown in the representative cross section presented in figure 2, taken from Ruskin (2006). They find

168 seismic sequences are physically continuous with the strata exposed, allowing for a multiproxy  
169 analysis of the sediments in sequence and for good age constraints on sequence deposition, using  
170 magnetostratigraphic and radiometric dating techniques. All but the lowest sequence (1 in figure 2)  
171 were deposited between 9 Ma and 4.3 Ma (Jordan *et al.*, 1997; Re *et al.*, 2003) and sequences younger  
172 than ~7 Ma were restricted to the west of the intrabasinal fault zone, highlighted in figure 2, as the  
173 basin narrowed. Younger strata, deposited in the basin, likely during a period of internal drainage,  
174 were evacuated to the Bermejo foreland < 2 Ma, as a through-going drainage system across the  
175 Precordillera was established (Val *et al.*, 2016). Today, four generations of alluvial fan terraces overlie  
176 a levelled Neogene surface in the proximal-medial piedmont (Perucca & Martos, 2012; Val *et al.*,  
177 2016). The alluvial terraces increase in thickness basin-wards, where Perucca and Martos (2012)  
178 report Quaternary sediments 0.1-3 m thick in the proximal-medial piedmont, thickening to 10 m in  
179 the distal piedmont. Continued uplift of the proximal piedmont is thought to have isolated the oldest  
180 exposed fan terrace (Perucca & Martos, 2012). These Iglesia basin terraces have not been dated,  
181 though Perucca and Martos (2012) suggest their chronology can be correlated with alluvial surfaces  
182 dated by Siame *et al.* (1997) on the eastern piedmont further south. Siame *et al.* (1997) provide  
183 cosmogenic dates for an oldest surface of ~ 770 kyr, where the youngest surface is ~ 40 kyr. There is  
184 no evidence for a significant change in uplift of the Frontal Cordillera through the Quaternary,  
185 therefore the structure of the basin is assumed stable up to present with only minor neotectonic  
186 faulting affecting mid-Quaternary surfaces in the east of the basin (Perucca & Martos, 2012).

187 Accumulation rates in the basin likely varied over time as sediment export to the foredeep occurred  
188 intermittently with the opening and closure of a through-going drainage system across the  
189 Precordillera (Suriano *et al.*, 2015). From <sup>10</sup>Be cosmogenic concentrations in sediments sampled  
190 upstream of the Iglesia basin, Val *et al.* (2016) derive paleo-erosion rates of ~ 0.1-0.25 mm/yr between  
191 7 and 5.2 Ma. These erosion rates are comparable to accumulation rates derived by Ruskin (2006)  
192 from magnetostratigraphy, where a marked decrease in accumulation from >10 m / 10kyr in the late  
193 Miocene uplift phase, to 0.1- 1 m / 10kyr in the Pliocene is observed. These latter rates are comparable

194 to regional millennial scale erosion rates for the Holocene (Bookhagen & Strecker, 2012; Carretier *et*  
195 *al.*, 2015).

196 Sediment transport events in the Iglesia basin today occur during infrequent summer storms linked to  
197 meteorological variations of the El Niño Southern Oscillation (ENSO), which drives irregular  
198 distributions of intense rainfall over the region. The impact of ENSO variability is evident in the  
199 Holocene sedimentary record of the Jachal River valley (Colombo *et al.*, 2000; 2009) and over prints  
200 lower amplitude fluctuations in aridity (Iriondo and Garcia, 1993). During these short-lived events,  
201 sediment transport on the Iglesia fans occurs via channelized flow (Perucca & Martos, 2012) within an  
202 unarmoured bed (Harries *et al.*, 2018).

203 In this study, we focus on three catchment-alluvial fans on the Frontal Cordillera margin of the Iglesia  
204 basin (figure 1). These fans are excellent candidates for investigating size-selective transport in natural  
205 alluvial systems for several reasons: firstly, gravel transported on these fans is lithologically-hard,  
206 potentially limiting the impact of clast abrasion on the gravel mass balance of the systems. The gravel  
207 is a mix of predominantly intrusive, extrusive and sedimentary rocks sourced from the Andean Frontal  
208 Cordillera, generally transported by stream-bed flow for up to 40 km from the mountain front. Typical  
209 abrasion rates for gravel essentially made of intrusive and extrusive rocks are  $< 1 \%$  mass-loss / km,  
210 equivalent to a fining rate  $\leq 0.3 \%$  / km, but we note that rates for sedimentary rocks may vary over  
211 orders of magnitude (Attal *et al.*, 2006; Attal & Lavé, 2009). We work here with the assumption that  
212 abrasion has a minimal influence on the grain size trends along the fans and later discuss this  
213 assumption in light of our data. Furthermore, these systems have not been heavily modified by human  
214 activity and the semi-arid climate means vegetation cover is minimal, eliminating an additional control  
215 on sediment transport that might otherwise influence grain size trends along the rivers.

216

217 The largest of the three fans, ~40 km in downstream length, is named fan 1 and drains into the centre  
218 of the basin. Two smaller fans, 2 and 3, are ~25 km in downstream length, are located south and north  
219 of fan 1, respectively. Each fan is fed by a primary catchment and between two and four tributary  
220 catchments of variable sizes (see also *Harries et al.*, 2018). Smaller tributary catchments that feed  
221 directly into the mainstream, introduce sediment in the uppermost reaches of the fan, while larger  
222 tributary catchments have confluences with the main channel up to half way down fan, with sediment  
223 transport distances comparable to that in the trunk stream. The river channels are incised  $\leq 2$  m along  
224 their length into a fan surface attributed to the early Holocene (Perucca & Martos, 2012), where the  
225 modern channels themselves are braided with a channel and gravel bar morphology (*Harries et al.*,  
226 2018).

### 227 3. Methods

228 We investigate the extent to which Holocene downstream grain size fining trends on three adjacent  
229 catchment-alluvial fan systems in the Iglesia basin reflect the predictions of extant grain size fining  
230 models (e.g. Fedele & Paola, 2007; Duller *et al.*, 2010). We evaluate whether the external boundary  
231 conditions of each system can be reliably reconstructed from quantitative inversions of their Holocene  
232 downstream grain size fining trends and rates and patterns of subsidence. Here, we use the term  
233 subsidence to denote the differential subsidence generated by plate flexure due to loading and  
234 tectonic uplift, which together control the spatial distribution of accommodation space in the basin.

235 Gravel size data collected along the three alluvial fans are used to characterise the profile of grain size  
236 fining from fan apex to toe (section 3.1). A 3D model of basin stratigraphy is developed for the Iglesia  
237 basin through the mapping of sequence boundaries, imaged in seismic data (section 3.2). This is used  
238 to constrain the spatial distribution of sediment extraction, which is required as a parameter in the  
239 *Fedele and Paola* (2007) self-similarity grain size fining model; from this we compare the modelled  
240 downstream distribution of gravel grain sizes compared to the fining profile measured in the field

241 (section 3.3). Finally, we adapt this fining model to incorporate lateral inputs from both tributaries and  
242 terrace recycling (section 3.4).

### 243 *3.1 Field data – Grain size*

244 Surface grain size distributions were measured on the alluvial fans in October 2015 and are also  
245 presented in *Harries et al.* (2018), where the self-similarity in these grain size distributions is reported.  
246 In this contribution, we instead focus on the controls on downstream fining in these deposits. These  
247 data were collected at ~3 km intervals along the length of each alluvial river traversing the three fans,  
248 where measurements were spaced so to avoid sampling within 1.5 km of tributary confluences (figure  
249 1). At each locality we measured the size distribution of gravel (> 2mm) exposed on the dry, riverbed  
250 surface, the depth of channel incision and recorded the lithology of each clast sampled (figure A1).  
251 We assume that sediment finer than 2 mm (i.e. sand) is not transported as bedload and omit the finer  
252 size fractions from our analysis. An analysis of the clast lithology data is presented in the Appendix.  
253 The size distribution of gravel was characterised from the point counting of 200 clasts from two  
254 photographs; where 100 clasts were sampled from each photograph using an equally spaced grid  
255 (spacing ~200 mm) to systematically select clasts (c.f. Attal & Lavé, 2006; Whittaker *et al.*, 2011; Dingle  
256 *et al.*, 2016). To account for the greater volumetric significance of larger clasts on the bed, we counted  
257 clasts that cover  $n$  grid nodes  $n$  times in line with Kellerhals and Bray (1971) and previous publications  
258 in this field (Whittaker *et al.*, 2011; D'Arcy *et al.*, 2017). To attain a sample that was spatially  
259 representative of each locality, bar and channel deposits were sampled individually and their size  
260 distributions subsequently merged into a single composite distribution (c.f. Bunte & Abt, 2001). The  
261 bars present were both medial and alternating channel bars. Patchiness in grain size within these  
262 structures was subtle and less prominent than the grain size variance between sites. The relative  
263 contributions of gravel bar and channel deposits at each site were scaled by in-situ field estimates of  
264 their relative percentage cover on the bed (c.f. Bunte & Abt, 2001).

265 An analysis of the precision and potential bias in our sampling approach is detailed in Harries et al.  
266 (2018). We determine the precision of locating accurate population statistics from a sample of 100  
267 clasts by extrapolating precision estimates from lognormal distributions with similar standard  
268 deviations from Rice and Church (1996). They estimate the median of the parent population can be  
269 located with an absolute precision of  $\pm 0.84$  mm. By performing a two-sample t-test on the log-  
270 transformed size distributions of the channel and bar samples at each locality, we identify that the  
271 logarithmic mean grain sizes are statistically different between bed structures at a significance level  
272 of 0.05, these statistics are included in the supplementary information. We therefore identify that  
273 calculating the mean of the composite distribution has the largest source of error in our dataset. To  
274 take this into account, we recalculate the composite distributions when the estimates of channel and  
275 bar proportions are altered by 10%. The mean values from these distributions define the upper and  
276 lower error bars on our measurements. Here we present the arithmetic mean grain size for each site  
277 downstream,  $\bar{D}_x$ , from which we calculate the rate of exponential downstream grain size fining as:

$$278 \quad \bar{D}_x = \bar{D}_0 e^{-\alpha x} \quad \text{Equation 5}$$

279 where  $\bar{D}_0$  is the predicted input mean grain size,  $X$  is the downstream distance in km, and  $\alpha$  is the  
280 fining exponent with units of  $\text{km}^{-1}$ . We calculate the coefficient of variation ( $C_v$ ) for each local grain  
281 size distribution as

$$282 \quad C_v = \frac{\sigma}{\bar{D}} \quad \text{Equation 6}$$

283 where  $\sigma$  is the standard deviation measured directly from the local size distribution. Studies suggest  
284 that deposits in which there is no spatial trend in  $C_v$  downstream are most suitable for the application  
285 of the self-similarity model of Fedele and Paola (2007) (e.g. Whittaker *et al.*, 2011; D'Arcy *et al.*, 2017).  
286 Harries *et al.* (2018) demonstrate the size distributions on all three fans are broadly self-similar and  
287 that there is no statistically significant change in  $C_v$  downstream, allowing us to confidently apply the  
288 Fedele and Paola (2007) self-similar solutions.

289            *3.2 Subsidence from seismic data*

290    We construct a 3D model of the Iglesia basins stratigraphy in Petrel™ using 2D seismic interpretations  
291    of basin fill obtained from Ruskin (2006). Up to six sequence boundaries, younger than 6.57 Ma, were  
292    traced across the seismic grid and used to construct isopach maps of basin fill through time. Neither  
293    geophysical nor petrographic information from well logs are freely available for the Iglesia basin,  
294    therefore, we convert two-way travel times (TWT) to true vertical depth (TVD) using a lithologically-  
295    appropriate reconstruction of the depth-velocity profile for the basin fill. At the surface, the Tertiary  
296    sandstones and shales exposed have a similar velocity range, 2-2.6 km/s (Ruskin, 2006), therefore we  
297    use a mean value of 2.3 km/s as a velocity at the surface and apply a compaction correction at 1 km  
298    depth intervals using a compaction profile published in figure 21.8 of North (1985). We attain a depth-  
299    averaged velocity of 2.8 km/s over 3 km of fill, in-line with previous inversions by Snyder (1988).

300    To test the assumption that the spatial distribution of subsidence has not changed significantly  
301    through time, we extract 2D cross sections, parallel to the alluvial fans sampled on the surface, and  
302    calculate the rate of subsidence of each sequence boundary using the available age constraints on  
303    deposition (i.e. depth/age). The oldest sequence boundary (sb) mapped, sb6, is detectable with high  
304    continuity and amplitude and is temporally well constrained in outcrop to 6.57 Ma (Ruskin, 2006). This  
305    boundary corresponds with the base of seismic sequence 6 in figure 2. The upper boundary of seismic  
306    sequence 6, sb7, is constrained to 5.23 Ma. Sequences younger than sb7 are not well dated, though  
307    the minimum age of sequence deposition is constrained to >4.3 Ma, based on magneto-stratigraphy  
308    (Ruskin, 2006). As four depositional sequences between sb7 and sb11 were deposited within <1Ma,  
309    uncertainty on the age of each sequence boundary is relatively low and comparable to the age  
310    uncertainty associated with the dated sequence boundaries. We therefore estimate the age of each  
311    of the youngest sequence boundaries assuming a constant rate of sediment accumulation and  
312    consider the difference between subsidence profiles of all sequence boundaries to be a function of  
313    change in the spatial pattern of accommodation space and uncertainty in accumulation rates through  
314    time.

315 As the seismic survey does not extend to the mountain front, we linearly extrapolate the profile of  
316 basin subsidence up to the first surface exposure of bedrock. We consider the error on our  
317 extrapolation using two linear, end-member scenarios. The first extrapolates to the easternmost  
318 bedrock outcrop at the front of the range, while the second extrapolates to the apex of fan deposition.

### 319 *3.3 Self-similar grain size fining model*

320 Our model formulation for solving the downstream distribution of grain sizes on an alluvial fan  
321 incorporates Fedele and Paola's (2007) self-similar solution for downstream fining of gravel. A  
322 complete derivation of this approach is described in Fedele and Paola (2007) and a modified field  
323 version is presented in Duller *et al.* (2010) (c.f. Whittaker *et al.*, 2011; D'Arcy *et al.*, 2017). Below we  
324 outline the points of our modelling procedure; a more detailed derivation is provided in the appendix.

325 We define the spatial distribution of tectonic subsidence,  $r$ , for each system as a 2D profile, extracted  
326 directly from the seismically-derived 3D subsidence model of sb 6, as described in section 3.2. For this,  
327 and the total downstream system length, we define the spatial distribution of deposition  
328 downstream,  $R^*(x^*)$  using equation 3. The sediment flux at any downstream distance,  $q(x^*)$ , is not  
329 defined explicitly but is a function of flux required to fill the accommodation space created by tectonic  
330 subsidence and the fraction of basin filling,  $\beta$ ; it is determined by solving  $q_{s0} = \beta \left[ (1 - \right.$   
331  $\left. \lambda_p) \int_0^{x^*} r^*(x^*) \right]$ . By including  $\beta$  we account for the basin being open, allowing sediment to bypass the  
332 fan system if the accommodation space is overfilled ( $\beta > 1$ ). This variable is an important control on  
333 the mass balance of the system (c.f. Paola & Martin, 2012). We compare  $q_s$  from the model solutions  
334 to first order estimates of sediment flux from the primary and tributary source catchments feeding  
335 the fans (figure 1), previously published in table 1 of Harries *et al.* (2018). These estimates were made  
336 using a BQART sediment flux model after Syvitski and Milliman (2007) and are ground-truthed against  
337 catchment-averaged cosmogenic denudation rate estimates for the region (Bookhagen & Strecker,  
338 2012; Carretier *et al.*, 2015). For further information see the supplementary material and Harries *et*  
339 *al.* (2018).



340 Assuming the evolution of the river long profiles are diffusional and have an exponential decay in grain  
 341 size downstream, a solution for gravel fining dependent on the distribution of  $R^*$  (as function of  $x^*$ )  
 342 can be obtained using the following transformation:

$$343 \quad y^*(x^*) = \int_0^{x^*} R^*(x^*) dx^* \quad \text{Equation 7}$$

344 where  $y^*$  integrates the distribution of  $R^*$  as a function of dimensionless distance downstream.  
 345 Fedele and Paola (2007) demonstrate that downstream fining profiles are invariant for a specific  
 346 distribution of  $y^*(x^*)$ , and thus, they show the mean grain size for gravels at any point downstream,  
 347  $\bar{D}(x^*)$ , can be expressed as an exponential function of  $y^*$  so that:

$$348 \quad \bar{D}(x^*) = \bar{D}_0 + \sigma_0 \frac{C_2}{C_1} (e^{-C_1 y^*} - 1) \quad \text{Equation 8}$$

349 where  $\bar{D}_0$  and  $\sigma_0$  are the mean and standard deviation of the input size distribution at  $x_0$  and  $C_1$  and  
 350  $C_2$  are constants that describe how the total grain size variance in the gravel supply is partitioned into  
 351 local site variation ( $C_1$ ) and variation down-system, which manifests as a downstream change in  
 352  $\bar{D}$  ( $C_2$ ). We define  $\bar{D}_0$  as the intercept of an exponential fining curve fit to the observed grain size data  
 353 and scale  $\sigma_0$  to  $\bar{D}_0$  using the average  $C_v$  measured downstream. Fedele and Paola (2007) demonstrate  
 354 that in a perfectly self-similar system, the partitioning of the variance into  $C_1$  and  $C_2$  does not depend  
 355 explicitly on  $x^*$  and therefore, can be solved analytically using  $\sigma$  and  $\bar{D}$  of gravel deposited at local  
 356 sites downstream.

$$357 \quad C_v = \frac{\sigma(x^*)}{\bar{D}(x^*)} = \frac{C_1}{C_2} \quad \text{Equation 9}$$

358 The  $C_v$  of self-similar deposits is typically found to lie between 0.7 and 1.0, as observed in field studies  
 359 (e.g. Fedele & Paola, 2007; Whittaker *et al.*, 2010; Michael *et al.*, 2013). Numerical models suggest  $C_1$   
 360 has a limited range and lies between 0.55 and 0.9 (Paola & Seal, 1995; Fedele & Paola, 2007).  
 361 Consequently  $C_2$  can be approximated. Previous studies have used intermediate values of  $C_1$ , i.e. 0.7,  
 362 (Duller *et al.*, 2010; D'Arcy *et al.*, 2017), although there are few independently-constrained estimates

363 of its value in the literature. In this study, we measure  $C_v$  from our field grain size data, and we use  $C_1$   
364 = 0.7, consistent with D'Arcy *et al.* (2017).

365 We first present the results from this model and compare the fit to the grain size data collected in the  
366 field. The model is then adapted to analyse the impact of lateral inputs of sediment on the grain size  
367 fining curves. The diagram in figure 3 depicts the modifications made to the model in order to replicate  
368 the processing of lateral sediment inputs in natural settings. The first adapted model, (the tributary  
369 model) is modified so that the sediment fill in the basin is not solely supplied by a single apex point  
370 source, but is partitioned between several tributary point sources. The distance downstream of each  
371 tributary confluence is measured from satellite imagery for the respective fan and is a fixed variable  
372 in the model. To avoid the necessity for quantitative constraint on the sediment supply from different  
373 inputs, we distribute 100% of the  $Q_s$  in each model run between the primary and tributary catchments  
374 using their ratios of BQART sediment supply estimates, reported in table A1 and *Harries et al.* (2018).  
375 As a first order approximation, this allows us to account for the relative size of each tributary  
376 catchment supplying sediment to the system. The second adapted model (the recycling model) mixes  
377 a sediment flux with a particular grain size distribution with the trunk-stream supply at each  
378 downstream node along the length of the system. This process replicates the continual addition of  
379 sediment into the modern system by river incision and surface reworking.

380 At each lateral input node, a mixing model incorporates an additional sediment flux with a self-similar  
381 grain size distribution, into the trunk-stream.

$$382 \quad \bar{D}_{mixed} = \bar{D}_m \left( \frac{Q_{s_m}}{Q_{s_m} + Q_{s_t}} \right) + \bar{D}_t \left( \frac{Q_{s_t}}{Q_{s_m} + Q_{s_t}} \right) \quad \text{Equation 10}$$

383 The mean grain size downstream of the input node,  $\bar{D}_{mixed}$ , is a function of the mean grain size and  
384 sediment flux upstream of the input,  $\bar{D}_m$  and  $Q_{s_m}$ , and the mean grain size and sediment flux in the  
385 tributary,  $\bar{D}_t$  and  $Q_{s_t}$ . The standard deviation of the mixed sediment supply,  $\sigma_{mixed}$ , is scaled to  
386  $\bar{D}_{mixed}$  using  $C_v$ . The profile of mass extraction downstream,  $y^*$ , is altered so that the spatial

387 distribution of deposition,  $R^*$ , is integrated from the downstream distance of each new lateral input  
 388 node,  $x_i^*$ .

$$389 \quad y^*(x^*) = \int_{x_i^*}^{x^*} R^*(x^*) dx^* \quad \text{Equation 11}$$

390 The profile of deposited grain sizes downstream of a lateral input is:

$$391 \quad \bar{D}(y^*(x^*)) = \bar{D}_{mixed} + \sigma_{mixed} \frac{C_2}{C_1} (e^{-C_1 y^*} - 1) \quad \text{Equation 12}$$

392 In the special case  $\bar{D}_{mixed} \approx \sigma_{mixed} \frac{C_2}{C_1}$  this reduces to a simple exponential

$$393 \quad \bar{D}(y^*(x^*)) = \sigma_{mixed} \frac{C_2}{C_1} e^{-C_1 y^*} \quad \text{Equation 13}$$

394 In this paper we introduce another possibility, i.e. that an exponential form can result even when the  
 395 criterion  $\bar{D}_{mixed} \approx \sigma_{mixed} \frac{C_2}{C_1}$  is not met. We refer to this as an ‘empirical’ exponential, where  $A$  is the  
 396 input grain size and  $B$  is fining exponent.

$$397 \quad \bar{D}(y^*(x^*)) = A e^{-B y^*} \quad \text{Equation 14}$$

398 We suggest that this form can occur as a consequence of the complexity of the system.

### 399 *3.4 Model analysis*

400 To analyse the sensitivity of the grain size fining trends observed in the field to changing boundary  
 401 conditions, we determine the range of model best fit solutions that could statistically describe the  
 402 measured data, each of which has an associated likelihood. We estimate the best fit of the theoretical  
 403 models of the form (12) or (14) to the measured data by calculating the log-likelihood function,  $\hat{l}$ , from  
 404 the residual sum of squares (RSS) for each hypothesis  $H(x) = f(x)$ . For each theoretical model, we  
 405 derive the maximum likelihood estimate,  $\hat{f}(x_i)$ , attained by varying parameters,  $k$ , to fit the model,  
 406  $y$ , to the measured data,  $x$ , with  $n$  data points.

$$407 \quad \hat{l} = -\frac{n}{2} \ln \left[ \sum_{i=1}^n \left\{ \left[ (y_i - \hat{f}(x_i))^2 \right] \right\} \right] = -\frac{n}{2} \ln(RSS) \quad \text{Equation 16}$$

408 The maximum likelihood solution for the model parameters is determined by fitting the measured  
409 data to the different hypotheses using a non-linear least squares regression. We then distinguish  
410 between the competing models using the likelihood ratio, calculated from the log-likelihood  
411 difference between the theoretical model,  $\hat{l}_2$ , and empirical exponential,  $\hat{l}_1$ .

$$412 \quad \hat{l}_2 - \hat{l}_1 = -\frac{n}{2} [\ln(RSS_2) - \ln(RSS_1)] \quad \text{Equation 17}$$

$$413 \quad \frac{L_2}{L_1} = \exp\{\hat{l}_2 - \hat{l}_1\} \quad \text{Equation 18}$$

414 The strength of the evidence for a preference or similarity between models 1 and 2 depends on the  
415 likelihood ratio ( $L_2/L_1$ ) (Kass & Raftery, 1995). Hypothesis 2 is formally indistinguishable from  
416 hypothesis 1 if  $L_2/L_1 \approx 0$ . Hypothesis 2 is preferred over hypothesis 1 when the likelihood ratio,  
417  $L_2/L_1$ , is equal to or greater than 1.  $L_2/L_1$  in the range of 1-3 has a preference for hypothesis 2 that  
418 is 'slight', 3-10 is 'substantial', 10-30 is 'strong' (Lee & Wagenmakers, 2014).

419 For the original model of Fedele and Paola (2007), with a single apex input of sediment, we derive a  
420 maximum likelihood best fit by systematically varying two broadly constrained variables within the  
421 model: the fraction to which the basin is filled,  $\beta$ , between 0.6 and 2.0, and the sediment transport  
422 coefficient,  $C_1$ , between 0.6 and 0.8. With the tributary model, we systematically vary the mean grain  
423 size of all lateral inputs,  $\bar{D}_t$ , between 2 and 80 mm, and the fill fraction, between 0.6 and 6. These  
424 ranges are sensible limits set by the range of gravel grain sizes we observed in the field and by  
425 sediment volumes that are plausible for the Iglesia basin based on estimates of catchment sediment  
426 fluxes (Harries *et al.*, 2018). The sensitivity of the fit to varying parameters is analysed in contour plots  
427 of the ratio of log-likelihood estimates,  $f(x)$ . We extract the model solutions that fall within 10% of  
428 the maximum likelihood best fit and rerun the model with these parameters fixed, varying a third grain  
429 size parameter; the mean grain size,  $\bar{D}_t$ , supplied by tributaries in the upper fan. For the recycling  
430 model, we vary three independent variables simultaneously: the mean grain size of the lateral inputs  
431 between 2 and 80 mm, the fill fraction, between 0.6 and 6, and the supply rate of recycled sediment,

432 which in this 2D model is scaled to rates of vertical incision, between 0.1 and 5 m / 10 kyrs. For both  
433 lateral input models, we consider a good fit to the data to fall within 10% of the maximum likelihood  
434 best fit, which roughly corresponds to solutions that produce a fining rate within one standard  
435 deviation of the best fit empirical model.

436 With this approach we highlight the range of model solutions that could statistically describe the  
437 observed grain size data. To quantify how tributary inputs and sediment recycling can buffer the  
438 sensitivity of grain size fining trends to changing boundary conditions, we experiment with altering  
439 the subsidence rate in the basin. We fix the free variables in the model with the best fit solution for  
440 the respective models and vary the subsidence rate in the basin by 0.5, 2 and 4 times the present rate  
441 to emulate a range of plausible scenarios for the Iglesia basin (Allmendinger *et al.*, 1990). We also  
442 investigate what profile of subsidence would be inverted from the grain size data using the original  
443 model when  $Q_s$  is constrained by sediment flux estimates from the BQART model and the basin is  
444 assumed 100% filled. The subsidence profile is given an exponential form with a wavelength set by  
445 the width of the basin and we experiment with changing the exponent of the solution. The results  
446 from these two experiments are presented in summary figures 9 and 10 and are discussed in section  
447 5.1.

## 448 4. Results

### 449 4.1 Basin subsidence

450 From the late Miocene to present, the locus of the maximum rate of subsidence in the Iglesia basin  
451 has been approximately 20-30 km from the mountain front. In figure 4, our 3D basin model indicates  
452 that the profile of subsidence varies considerably along strike of the front. For all six sequence  
453 boundaries (sb) analysed, isopachs highlight two subsidence centres, north and south of the basin axis  
454 (Appendix figure A3). Maximum subsidence is focused south of the basin axis, where sb6 (6.57 Ma)  
455 and sb7 (> 4.3 Ma) reach depths of 2000 m and 1400 m (figure 4), respectively. From this depo-centre,  
456 subsidence decreases rapidly toward the southern basin margin, where seismic sequences onlap

457 Palaeozoic basement. North of the basin axis, the pattern of subsidence is broader, where sb6 plateaus  
458 around depths of 1500-1700 m and sb10, around 800-900 m. The northern margin of the basin is not  
459 imaged. Uplift on the south eastern margin of the basin correlates in space to the footwall of a positive  
460 flower structure, associated with the northern termination of the El Tigre strike slip fault system  
461 (figure 2).

462 The pattern and rate of subsidence through time in transects parallel to our measurement sites is  
463 examined in 2D cross sections in figure 5. There is a broad agreement between the amplitude and  
464 shape of the subsidence profiles derived for dated sb 6 and 7 for each respective fan. Fan 2 has the  
465 highest rate of subsidence  $2.25 \pm 0.1$  m/ 10 kyr at its toe, ~25 km downstream from the fan apex. Fan  
466 3 has a shallower subsidence profile that plateaus ~ 18 km downstream from the fan apex to the fan  
467 toe with a maximum rate of subsidence of  $1.55 \pm 0.05$  m/ 10kyr. The maximum rate of subsidence on  
468 fan 1 is  $1.8 \pm 0.1$  m/10 kyr and is located ~30 km from the fan apex. As fan 1 is longer than the other  
469 two fans, we observe subsidence decreasing downstream toward the toe to 1.2 m/10 kyr. The younger  
470 sequence boundaries, 8-11 also have a similar wavelength of subsidence and if we assume constant  
471 sedimentation rate through time, we find the maximum difference in the rate of subsidence between  
472 all sequence boundaries is relatively small; 0.2-0.5 m/10 kyr for all fans. In the absence of any evidence  
473 suggesting a marked change in subsidence through time, we conclude that the rate and pattern of  
474 subsidence has remained the same since the Late Miocene and we apply the subsidence profile of sb  
475 6 as a boundary condition for Quaternary deposition in our model.

476 The amount of accommodation space produced by subsidence, calculated from a 2D area integration  
477 of the subsidence profile for sb 6, is estimated ~8500, ~9300 and 7600 m<sup>2</sup>/ 10 kyr for fan 2, fan 1 and  
478 fan 3, respectively. This is the space made available for mass extraction within the self-similar fining  
479 model. Assuming 30 % porosity for gravel in the basin fill (Allen & Allen, 2013), the average  
480 accumulation rates required to fill the accommodation space are ~0.65, 0.60 and 0.53 m/ 10 kyr, for  
481 fans 1, 2 and 3, respectively. These estimates are in line with accumulation rates derived by Ruskin

482 (2006) from magnetostratigraphy of basin fill outcrops exposed in the east of the basin, which suggest  
483 average millennial accumulation rates of <1 m/ 10 kyrs for the early Pliocene.

## 484 *4.2 Modelling grain size fining*

### 485 *4.2.1. Empirical model*

486 The mean grain size of river bed sediment measured at site 1, taken to be the input mean grain size  
487 at  $X_0$ , is 93 mm on fan 1, 164 mm on fan 2 and 119 mm on fan 3 (table 1). Downstream, the mean  
488 grain size fines exponentially with exponents of 1.8 % / km on fan 1, 6.7 % / km on fan 2 and 5.9 % /  
489 km on fan 3. These fining rates are an order of magnitude greater than would be expected from  
490 abrasion alone for our resistant lithologies (Attal *et al.*, 2006; Attal & Lavé, 2009), supporting our  
491 assumption that abrasion is not the main control on sediment fining across the studied fans. These  
492 fining rates are the same order of magnitude as those measured in Eocene Pablo basin, Spanish  
493 Pyrenees (Whittaker *et al.*, 2011) and Holocene fans in Death Valley (D'Arcy *et al.*, 2017). They are an  
494 order of magnitude greater than would be expected from abrasion alone for extrusive and intrusive  
495 gravel, typically less than 0.3 % / km (Attal *et al.*, 2006; Attal & Lavé, 2009). However, because our  
496 gravel contains a significant proportion of sedimentary rocks, we have to assess whether the  
497 preferential abrasion of sedimentary rocks could lead to such downstream fining. The analysis  
498 presented in Appendix A2 shows that the influence of abrasion is likely minimal on fans 2 and 3,  
499 therefore supporting our initial assumption, but that abrasion may contribute to a maximum of 30 %  
500 of the downstream fining on fan 1. For simplicity, we focus in the following on the potential influence  
501 of tributary input and recycling on grain size trends, and present results that do not account for  
502 abrasion. We highlight that the influence of abrasion should be considered in cases where the  
503 sediment transported on fans is highly erodible. In the case of fan 1, we note that not taking into  
504 account the effect of abrasion may lead to an overestimating of the volumes of sediment required to  
505 fit the data, but the overall patterns and interpretations are not affected.

506 On figure 6, we highlight 95% ( $2\sigma$ ) and 68% ( $\sigma$ ) confidence bounds for the non-linear least squares  
507 regression of the exponential to the measured data. Scatter in mean grain size of fan 1's upper reach  
508 reduces the confidence of the exponential fit to the data; this is reflected in a relatively high RMSE of  
509 12.07 and a  $\hat{l}_1$  of 7.29. An exponential model fit to fan 2's data has a RMSE of 23.02, a  $\hat{l}_1$  of 8.35 and  
510 wide confidence intervals. Fan 3's regression has a RMSE of 7.17, a  $\hat{l}_1$  of 6.02, and narrow confidence  
511 bands, reflecting the limited scatter in the dataset and the excellent fit of an exponential function.

#### 512 *4.2.2. Single source model*

513 The 2D model solution for a system with a single apex input of sediment predicts (after Fedele & Paola,  
514 2007) for all fans, that the mean grain size fines slowly from the fan apex across the upper reach of  
515 the fan, and then fines rapidly in the lower reaches, producing a convex fining profile (red lines, figure  
516 6). This trend is fundamentally driven by the fact that accommodation space is limited in the upper  
517 reaches of the fans and increases markedly down fan toward the basin centre (figure 5), leading to  
518 increasing rates of sediment extraction and increased fining down-fan. Under no sediment supply or  
519 bedload mobility scenario can the single apex model reproduce the exponential pattern of grain size  
520 fining observed in the field, as demonstrated in figure 6.

#### 521 *4.2.3. Tributary model*

522 Tributary catchments are estimated to supply 46% of the total sediment flux to fan 1 (table A1). We  
523 find that for the first iteration of the model, a mean tributary input grain size of 60 mm and a basin  
524 that is over supplied with sediment ( $\beta = 2$ ) produces a likelihood ratio of 0.35 and is therefore  
525 indistinguishable from the empirical model (figure 7a). The maximum likelihood ratio of 5.5 is achieved  
526 when the grain size of the upper fan tributaries is allowed to vary independent of the down fan  
527 tributaries, showing that the tributary model fits better than the empirical exponential model. This  
528 best fit solution has a fine, ~20 mm, tributary input in the upper fan and a coarse, 60 mm, input in the  
529 lower fan (figure 7a (ii)). However, solutions that have a likelihood ratio  $> 1$  also show a preference for  
530 the tributary model over the empirical model (eq. 14) and fall within  $1\sigma$  error of the latter model.



531 These solutions, plotted in plot 7a (i), can be generated for a moderate range of basin fill fractions,  
532 2.0-6.0, and tributary grain sizes <50 mm. By distributing the two sediment input points downstream,  
533 the tributary model can, therefore, produce a grain size fining profile that is statistically similar to that  
534 observed in the field for a number of basin fill and input grain size scenarios. Although we do not have  
535 detailed grain size data for these lateral inputs, the values predicted are consistent with the types of  
536 grain size supplied by catchments in this area (Harries *et al.*, 2018).

537 Tributaries supply 68% of the total catchment flux to fan 3, in two main locations. Contour plot c (ii)  
538 in figure 7 shows a maximum likelihood ratio of 0.4 is attained for the best fit solution where the basin  
539 is slightly over-filled ( $\beta = 1.2$ ) and the lateral input mean grain size is  $\sim 40$  mm (first iteration). The  
540 likelihood ratio is not improved by varying the grain size of different tributaries independently (second  
541 iteration). The tributary model is indistinguishable from the empirical model in this case. Solutions  
542 with likelihood ratios  $> 0$  also fall within  $2\sigma$  of the empirical model and are plotted as downstream  
543 fining curves in figure 7c (i). These solutions cover a range of basin fill fractions, 0.8-1.5, and grain  
544 sizes, <70 mm.

545 Fan 2's grain size fining profile cannot be effectively reproduced using the tributary model. As shown  
546 in plot 7b, the best fit solution deviates little from the single apex model solution. There is a clear  
547 preference for the empirical model with a likelihood ratio of  $10^{-4}$ . This is due to the fact that the main  
548 tributary input occurs at  $> 10$  km downstream and contributes only 18% of the total catchment supply,  
549 a flux that is evidently too small to have a significant impact on the grain size fining profile, irrespective  
550 of the grain size of the lateral input.

#### 551 *4.2.4. Recycling model*

552 The recycling model applied to fan 1 achieves a maximum likelihood ratio of 0.9, indicating the  
553 recycling model is indistinguishable from the empirical exponential (figure 8a (ii)). As with the tributary  
554 model, the best fit to the measured data is attained with a coarse mean lateral input grain size of 60  
555 mm (figure 8a (ii)). The rate of incision that best fits the data is between 3 and 4 m / 10 kyr. However,

556 in plot 8a (i) we show model solutions that have a likelihood ratio  $> 0.1$  also fall within a  $1\sigma$  error of  
557 the empirical model, which encompasses a wide range of possible rates of incision,  $0.1 - 5$  m / 10 kyr,  
558 and the full range of grain sizes tested. We do not have extensive grain size measurements of the fan  
559 surfaces being incised, however the range of grain sizes predicted by the model were observed both  
560 on the terrace surfaces and in cross-section.

561 A statistical fit to fan 3's grain size fining profile is also indistinguishable from the empirical model with  
562 a maximum likelihood ratio of 0.6 (figure 8c (ii)). A best fit to the data is attained with 1 m / 10 kyr of  
563 incision and the recycling of gravel with a mean grain size of 2 mm in a basin that is 100% filled ( $\beta=1$ ).  
564 Solutions with a likelihood ratio  $> 0.05$  fall within  $1\sigma$  error of the empirical model, plotted in figure 8c  
565 (i), and are well constrained to a narrow range of grain sizes,  $<30$  mm, and incision rates,  $0.1-2.5$  m /  
566 10 kyr.

567 For fan 2, the recycling model produces a fit with a maximum likelihood ratio of 1.4 and is therefore  
568 slightly preferred over the empirical model (figure 8b (ii)). As with fan 3, the best fit solution has a  
569 mean lateral input grain size of 2 mm and 1 m / 10 kyr of channel incision. However, solutions with a  
570 likelihood ratio of  $> 0.2$  fall within  $1\sigma$  error of the empirical model, plotted on figure 8b (i), and are  
571 attained for the full range of recycled fluxes and basin fill fractions tested.

## 572 5. Discussion

573 With unique constraints on the subsidence profile of the Iglesia basin and therefore the time-  
574 integrated distribution of mass extraction downstream, we have demonstrated that a classical 2D  
575 single source self-similarity grain size fining model (Fedele & Paola, 2007) cannot reproduce observed  
576 rates of downstream sediment fining in the modern rivers that deliver material to the alluvial fans  
577 filling the Iglesia basin. We show that from fan apex to toe, the mean grain size of gravel deposited on  
578 the river bed of each fan decreases exponentially. This reduction in grain size primarily occurs in the  
579 upper reaches of each fan, despite there being little accommodation space to drive a reduction in  
580 sediment calibre by size-selective mass extraction. However, by developing our grain size model to

581 include lateral inputs of sediment, we show additional sediment supplied downstream of the apex  
582 source can markedly modify the spatial distribution of mass supplied to the sediment routing system  
583 and alter the profile of downstream grain size fining.

584 Lateral inputs of sediment have been considered a source of noise in downstream grain size trends  
585 (Knighton, 1980; Hoey & Bluck, 1999; Gomez *et al.*, 2001) and there is certainly evidence of this on the  
586 Iglesia basin fans where tributary confluences correlate in space with substantial fluctuations in mean  
587 grain size. While we aimed to limit the impact of local slope and grain size variability at tributary  
588 confluences by sampling at distance from the input, autogenic adjustments of the bed surface slope  
589 to local fluctuations in water discharge, sediment flux and grain size may impact local grain size  
590 variability. Furthermore, a lack of synchronicity between sediment transport events in the main  
591 stream and channel may bias sampling toward more recent events. This transient variability  
592 introduces scatter in the downstream grain size fining profiles and reduces the sensitivity of the model  
593 fit to the data. For example, a greater scatter in the dataset of fan 1 compared to fan 3 means a larger  
594 combination of free parameters can be used to fit to the measured data, thereby reducing the  
595 effective sensitivity of the modelling. Importantly, however, we demonstrate when we consider  
596 transient, local variability in grain size as only a source of scatter in the grain size profiles of  
597 depositional systems, we find lateral inputs, defined by their flux and grain size alone, have a  
598 significant influence on the long term mass balance of the depositional system and their downstream  
599 grain size fining trends. Lateral sediment inputs can therefore be a driver of downstream fining.

600 With the tributary model, we find the profile of grain size fining can be modified by lateral inputs but  
601 only if the sediment flux from the input is relatively large and the grain size of the input is dissimilar  
602 to that of the trunk stream. For example, on fan 2, only 18 % of the total catchment flux is supplied by  
603 tributaries with little impact on the grain size fining trend, irrespective of input calibre. In contrast,  
604 tributaries supply fans 1 and 3 with 46 % and 68 % of their total catchment supply, respectively, which  
605 is a large enough to modify the grain size fining profile. As point sources, tributaries can create steps

606 in the grain size fining profile that emulate changes in the measured profile downstream of  
607 confluences (Rice 1998; 1999). A good statistical fit to the measured fining trends on these fans can  
608 be achieved with the addition of medium sized gravel in the upper fan. This finer input is necessary in  
609 order to induce fining on a reach with minimal subsidence. The best fit solution for fan 1 additionally  
610 requires tributaries further downstream to introduce large fluxes of coarse gravel, in order to maintain  
611 the very low rates of grain size fining observed. These sediment flux scenarios are in broad agreement  
612 with the first order estimates of sediment fluxes made by Harries et al. (2018) using a BQART model  
613 (table A1). The source catchments of fans 3 are estimated to supply  $\sim 12,000 \text{ m}^2 / 10 \text{ kyr}$  of sediment,  
614 which is comparable to the flux of sediment predicted by the fining model,  $16,000 \pm 5500 \text{ m}^2 / 10 \text{ kyr}$ .  
615 For fan 1, the fining model predicts sediment fluxes  $>38,000 \text{ m}^2 / 10 \text{ kyr}$  provide a good fit to the grain  
616 size data, which is larger than that estimated by the BQART model,  $\sim 25,000 \text{ m}^2 / 10 \text{ kyr}$ . Here it should  
617 be recognised that although these BQART estimates are in line with cosmogenic erosion rates derived  
618 for the region, they are subject to major uncertainties with regards to the proportion of the flux that  
619 is transported as bedload (Harries *et al.*, 2018).

620 Unlike the tributary model, the recycling model reproduces a smooth exponential fit to the data as  
621 sediment is supplied continuously downstream. The recycling of old fan surfaces is evident in the field  
622 (figure 1) and our modelling suggests these lateral inputs alone could account for deviations in the  
623 grain size fining profiles for all three fans. The best fit model solutions for fans 1 and 3, however, are  
624 similar to the tributary model solutions; fan 1 requires a large input of coarse sediment to maintain its  
625 low rate of grain size fining, whereas the smaller fans 2 and 3 require a small input of fine gravel to  
626 initiate fining in the upper fan. A flux of predominantly fine gravels onto the bed surface could arise if  
627 the recycled surface is enriched in finer gravels relative to the Holocene catchment supply, or equally,  
628 if the surfaces are similar in size composition but the Holocene discharge regime is less competent in  
629 transporting the same coarse size distribution. With no constraint on the flux of recycled material  
630 supplied to the model, we find the best fit solutions for fans 2 and 3 involve a rate of vertical incision  
631 into older fan surfaces of  $\sim 1 \text{ m} / 10 \text{ kyr}$ , which approximates the average channel depth in a Holocene

632 surface measured in the field (figure 1). This ground-truthing of the model results gives strength to  
633 our model outcomes being reasonable. The recycling solution for fan 1 indicates a rate of vertical  
634 incision of 4-5 m / 10 kyr is required to sustain the low rate of downstream grain size fining observed.  
635 Unlike fans 2 and 3, fan 1 is currently incising into a series of older generation surfaces; lack of good  
636 age constraints on these surfaces does not allow us to support or reject this model solution. It is likely,  
637 however, that both tributaries and the recycling of sediment, contribute to the exponential  
638 downstream fining trends on fans 1 and 3 and that one end member solution does not fully capture  
639 the sediment dynamics of the system (eq.13).

640 As well as being sensitive to the flux and calibre of lateral inputs, the fining profile is also controlled  
641 by the filled state of the basin or, alternatively, the percentage flux that bypasses the basin. The gravel-  
642 sand transition is typically correlated with downstream distance at which the bedload supply of gravel  
643 is exhausted, and is a good indicator of basin fill. For both lateral input models, best fit solutions for  
644 the smaller fans 2 and 3 indicate the basin is approximately filled. These solutions are in agreement  
645 with the fact that we observed a clear gravel-sand transition on both of the fans, which we use as a  
646 marker for the maximum downstream distance of the fan. We do not observe a gravel-sand transition  
647 on the largest fan 1 and, instead, mark the maximum downstream distance as the confluence of its  
648 main channel with the axial drainage system. With no apparent exhaustion of the gravel supply before  
649 this distance, there is evidence to suggest large fluxes of gravel are bypassing the fan. This is supported  
650 by the absence of any significant tributary mouth accumulations that would otherwise indicate  
651 sediment storage upstream. In line with these observations, our best fit model solutions for fan 1  
652 suggest this system has a catchment supply that is at least twice of what can be stored in the basin,  
653 implying that at least 50% of its catchment supply of gravel is bypassing the basin.

#### 654 *5.1 Sensitivity to external boundary conditions*

655 Using 2D self-similar models, we demonstrate lateral inputs of sediment in large alluvial systems are  
656 an important driver of downstream grain size fining as demonstrated in the Iglesia basin where we

657 can observe grain size fining in the upper reaches of three alluvial fans despite little available  
658 accommodation space to drive selective mass extraction. From our data, we find the downstream  
659 fining trends on each of the Iglesia basin fans can be explained if they are considered an integrated  
660 signal of both the catchment and fan responding to Holocene environmental change. This implies an  
661 external boundary condition change could be masked by dynamic depositional responses to forcing.  
662 Using the recycling model we explore whether grain size fining trends might still be sensitive to  
663 subsidence forcing in spite of signal masking. Here we assume that a change in subsidence rate is not  
664 accompanied by a change in the rate or character of sediment recycled and there is no alteration in  
665 how the drainage network of channels is configured. In summary figure 9a-c, a halving of the  
666 subsidence rate does not produce a fining curve that is statistically dissimilar from the modern  
667 subsidence rate. As our modelling predicts that the basins are at least filled and likely overfilled at  
668 present, a decrease in accommodation space for the same sediment supply would result in a greater  
669 rate of sediment bypass and a fining curve relatively insensitive to any excess of sediment. This loss of  
670 sensitivity to greater basin fill fractions was originally highlighted in Duller *et al.* (2010) and is clearly a  
671 major control on fining in the Iglesia basin. A quadrupling of the subsidence rate does provide a profile  
672 of grain size fining that is statistically different from the modern profile. Fining occurs more rapidly  
673 and, on all fans, the gravel supply is exhausted upstream of the modern fan toe. The effect is most  
674 pronounced on fan 1 where an under-filling of the basin has resulted in a gravel runout distance that  
675 is ~40% shorter than the modern system, equivalent to ~15 km of gravel retreat. On fans 2 and 3, the  
676 gravel runout distance is ~20% shorter than the modern system, equivalent to ~5 km of gravel retreat.  
677 This suggests that downstream grain size fining profiles, although buffered, can still be sensitive to  
678 changes in their boundary conditions that are of sufficient magnitude and in the right direction (i.e.  
679 towards greater subsidence).

## 680 *5.2 Wider implications and future work*

681

682 This work highlights the importance of both the tectonic boundary conditions and the locus of  
683 sediment inputs on the spatial distribution of mass extraction in a basin. It is therefore important to  
684 ask whether sediment recycling and tributaries are a source of “noise” in downstream grain size fining  
685 trends, or whether they are an important part of the signal. We argue that inversions of downstream  
686 fining profiles require us to consider the entire sediment routing system and its response to forcing,  
687 and not just the trunk stream. This approach better captures how the complex response of Quaternary  
688 alluvial fans to climatic change, where fan surface generation, abandonment and incision is typically  
689 observed, manifests in the geological record (Malatesta *et al.*, 2018).

690 This line of thinking also raises an important question: what should be considered the source of  
691 sediment in source-to-sink sediment routing models? Single apex models are not capable of describing  
692 the complexity of sediment sourcing dynamics in these large alluvial systems. The volumes of  
693 sediment recycled from Holocene fan surfaces can be comparable if not greater than the volumes  
694 supplied by catchments alone (D’Arcy *et al.*, 2017; Harries *et al.*, 2018), demonstrating that alluvial  
695 piedmonts are themselves important sources of sediment at least over intermediate timescales ( $10^2$ -  
696  $10^3$  years). Beyond the implications for quantitative reconstructions of basin stratigraphy, this sourcing  
697 problem also has an important inference for provenance studies using river bed gravels to reconstruct  
698 source region dynamics and for the application of cosmogenic nuclides in dating surface exposures  
699 and calculating catchment average erosion rates (Nichols *et al.*, 2005; von Blanckenburg, 2006;  
700 Wittmann *et al.*, 2011; Covault *et al.*, 2013; Foster *et al.*, 2017; Mason & Romans, 2018). These  
701 approaches typically rely on an assumption that the population of gravel in a stratigraphic horizon or  
702 bed surface is deposited instantaneously on a geological time frame, whereas we find the river bed  
703 surface is likely a recycled mixture of sediment cascading through the depositional realm over time.

704 In terms of reconstructing environmental boundary conditions from deposited grain sizes, the extent  
705 to which the spatial distribution of tectonic subsidence or the sediment budget of the system may be  
706 over or under-estimated by a lack of constraint on lateral sediment supplies needs to be considered

707 (c.f. Allen, 2008; Duller *et al.*, 2010; Armitage *et al.*, 2011; Allen *et al.*, 2013). The magnitude of  
708 sediment recycling and the geographical stability of tributary inputs over geological time-frames are  
709 variables that are important to constrain, though they are often unknowable for the geological past.  
710 Without this constraint, we have demonstrated inversions of basin structure and evolution could  
711 deviate significantly from reality. The two lateral input end member models newly developed in this  
712 study simplify the geomorphology of each system to include lateral inputs that are spatially uniform  
713 or point source specific. These models fall short of capturing the full spatial complexity of lateral  
714 sediment addition, however, they highlight the importance of considering lateral sediment input in  
715 models of sediment routing. Ground-truthing of the model results, with measurements of the grain  
716 size supplied by tributaries and recycled material, would corroborate whether the end member  
717 models do a good job at simplifying the geomorphology of the system.

## 718 6. Conclusions

719

720 With unique constraint on the external boundary conditions for sediment deposition in the Iglesia  
721 basin, we show how lateral sediment inputs exert a first order control on the profile of grain size fining  
722 in alluvial fan systems. For the three alluvial fans studied here, seismic mapping of dated sequence  
723 boundaries reveals subsidence increases away from the mountain front and along strike of the  
724 mountain front, with maximum rates of subsidence of 2.25 m / 10 kyr in the south and 1.55 m / 10 kyr  
725 in the north. Using a self-similar downstream grain size fining model constrained with measured  
726 subsidence profiles, we find we cannot reconstruct the profile of downstream grain size fining  
727 measured on the active river bed of each fan for any sediment supply scenario using a point source at  
728 the apex of the fans. This is because we observe fining in the upper fan where the model predicts  
729 downstream fining ought to be minimal due to the limited amount of accommodation space required  
730 to induce deposition. However, we develop the self-similarity model to incorporate bedload mixing  
731 and we demonstrate lateral inputs of sediment are key for replicating the Holocene grain size profiles  
732 on all fans.



733 We simplify the spatial variability in lateral inputs to two end-member models, a tributary model,  
734 adapted with two free parameters in the fraction of basin fill and the mean grain size of the lateral  
735 input, and a sediment recycling model, adapted with three free parameters in the fraction of basin fill,  
736 the recycled flux and the mean grain size of recycled material. For fans 1 and 3, the tributary model  
737 can produce profiles of grain size fining that provide a better fit or a fit indistinguishable from an  
738 empirical exponential model. These two fans have tributary fluxes that make up > 46 % of the total  
739 catchment sediment supply, which contrasts with fan 2, whose tributaries supply ~ 18 % of the total  
740 catchment flux. Here, the tributary model does not provide a better fit than the single input model for  
741 fan 2 as its tributary contributions are too small. The best fit solution for fan 1 requires coarse gravel,  
742  $\bar{D} \sim 60$  mm, to be supplied by the lower tributaries and fine gravel,  $\bar{D} \sim 20$  mm, to be supplied by the  
743 upper tributaries, and for the basin to be over filled ( $\beta \geq 2$ ). Data from fan 3 are best fit with an  
744 addition of medium gravel,  $\bar{D} \sim 40$  mm, and a basin slightly over filled ( $\beta = 1.2$ ). The recycling model  
745 provides a better fit or a fit indistinguishable from an empirical exponential model for all three fans.  
746 Both fans 2 and 3 are best fitted with a moderate flux of recycled fine gravel ( $\bar{D} \sim 2$  mm), equivalent  
747 to incision rates of 1 m / 10 kyr, consistent with field observations. The best fit solution for fan1  
748 requires a large flux of coarse gravel ( $\bar{D} \sim 60$  mm), equivalent to incision rates of 3-4 m / 10 kyr. The  
749 range of lateral input model solutions that can fit the data to within  $1\sigma$  of the exponential rate of  
750 downstream fining increases as scatter in the data increases. The sensitivity of the fit to varying the  
751 free parameters in the lateral input models is, therefore, relatively low for fan 1 (RMSE = 12.07), but  
752 high for fan 3 (RMSE = 7.17).

753 This relatively simple approach to incorporating complex sediment sourcing dynamics into grain size  
754 fining models has significant implications for how we interpret climatic and tectonic forcing from  
755 stratigraphic grain size trends. Fining trends are a predictable function of basin accommodation and  
756 sediment flux, but this sensitivity is masked by the complexity of sediment sourcing dynamics within  
757 the depositional basin. Quantitative inversions of large alluvial systems therefore need to consider  
758 lateral inputs of sediment as a major control on grain size fining, as grain size fining model solutions

759 which assume a single sediment source input may wrongly predict sediment fluxes or tectonic  
760 subsidence distributions in circumstances where lateral inputs drive down-system grain size profiles.

## 761 Acknowledgments

762

763 We thank Trevor Hoey and Julieta Suriano for their insightful reviews that helped improve the  
764 manuscript. This work was funded by NERC E<sup>3</sup> DTP Studentship NE/L002588/1 and The School of Geosciences  
765 at The University of Edinburgh.

## 766 References

767

- 768 ALLEN, P.A. & DENSMORE, A.L. (2000) Sediment Flux from an Uplifting Fault Block. *Basin Research*, **12**,  
769 367-380.
- 770 ALLEN, P.A. (2008) From Landscapes into Geological History. *Nature*, **451**, 274-276.
- 771 ALLEN, P.A. & HELLER, P.L. (2012) Dispersal and Preservation of Tectonically Generated Alluvial Gravels  
772 in Sedimentary Basins. *Tectonics of Sedimentary Basins: Recent Advances*, 111-130.
- 773 ALLEN, P.A. & ALLEN, J.R. (2013) *Basin Analysis: Principles and Application to Petroleum Play Assessment*,  
774 3rd edition edn. Wiley.
- 775 ALLEN, P.A., ARMITAGE, J.J., CARTER, A., DULLER, R.A., MICHAEL, N.A., SINCLAIR, H.D., WHITCHURCH, A.L. &  
776 WHITTAKER, A.C. (2013) The Qs Problem: Sediment Volumetric Balance of Proximal Foreland  
777 Basin Systems. *Sedimentology*, **60**, 102-130.
- 778 ALLEN, P.A., MICHAEL, N.A., D'ARCY, M., RODA-BOLUDA, D.C., WHITTAKER, A.C., DULLER, R.A. & ARMITAGE, J.J.  
779 (2017) Fractionation of Grain Size in Terrestrial Sediment Routing Systems. *Basin Research*,  
780 **29**, 180-202.
- 781 ALLMENDINGER, R.W., FIGUEROA, D., SNYDER, D., BEER, J., MPODOZIS, C. & ISACKS, B.L. (1990) Foreland  
782 Shortening and Crustal Balancing in the Andes at 30-Degrees-S Latitude. *Tectonics*, **9**, 789-809.
- 783 ALVAREZ-MARRON, J., RODRIGUEZ-FERNANDEZ, R., HEREDIA, N., BUSQUETS, P., COLOMBO, F. & BROWN, D. (2006)  
784 Neogene Structures Overprinting Palaeozoic Thrust Systems in the Andean Precordillera at 30  
785 Degrees S Latitude. *Journal of the Geological Society*, **163**, 949-964.
- 786 AMANTE, C. & EAKINS, B.W. (2009) Etopo1 1 Arc-Minute Global Relief Model: Procedures, Data Sources  
787 and Analysis. N. T. M. N. NGDC-24. National Geophysical Data Center, NOAA.
- 788 ARMITAGE, J.J., DULLER, R.A., WHITTAKER, A.C. & ALLEN, P.A. (2011) Transformation of Tectonic and  
789 Climatic Signals from Source to Sedimentary Archive. *Nature Geoscience*, **4**, 231-235.
- 790 ATTAL, M. & LAVÉ, J. (2006) Changes of Bedload Characteristics Along the Marsyandi River (Central  
791 Nepal): Implications for Understanding Hillslope Sediment Supply, Sediment Load Evolution  
792 Along Fluvial Networks, and Denudation in Active Orogenic Belts. *Tectonics, Climate, and  
793 Landscape Evolution*, **398**, 143-171.
- 794 ATTAL, M., LAVE, J. & MASSON, J.P. (2006) New Facility to Study River Abrasion Processes. *Journal of  
795 Hydraulic Engineering-Asce*, **132**, 624-628.
- 796 ATTAL, M. & LAVÉ, J. (2009) Pebble Abrasion During Fluvial Transport: Experimental Results and  
797 Implications for the Evolution of the Sediment Load Along Rivers. *Journal of Geophysical  
798 Research-Earth Surface*, **114**.
- 799 ATTAL, M., MUDD, S.M., HURST, M.D., WEINMAN, B., YOO, K. & NAYLOR, M. (2015) Impact of Change in  
800 Erosion Rate and Landscape Steepness on Hillslope and Fluvial Sediments Grain Size in the  
801 Feather River Basin (Sierra Nevada, California). *Earth Surface Dynamics*, **3**, 201-222.

802 BEER, J.A., ALLMENDINGER, R.W., FIGUEROA, D.E. & JORDAN, T.E. (1990) Seismic Stratigraphy of a Neogene  
803 Piggyback Basin, Argentina. *Aapg Bulletin-American Association of Petroleum Geologists*, **74**,  
804 1183-1202.

805 BOOKHAGEN, B. & STRECKER, M.R. (2012) Spatiotemporal Trends in Erosion Rates across a Pronounced  
806 Rainfall Gradient: Examples from the Southern Central Andes. *Earth and Planetary Science  
807 Letters*, **327**, 97-110.

808 BUFFINGTON, J.M. & MONTGOMERY, D.R. (1997) A Systematic Analysis of Eight Decades of Incipient  
809 Motion Studies, with Special Reference to Gravel-Bedded Rivers. *Water Resources Research*,  
810 **33**, 1993-2029.

811 BUNTE, K. & ABT, S.R. (2001) Sampling Surface and Subsurface Particle-Size Distributions in Wadable  
812 Gravel-and Cobble-Bed Streams for Analysis in Sediment Transport, Hydraulics and Stream  
813 Bed Monitoring, Gen. Tech Rep. Rms-Gtr-74, United States Department of Agriculture, Forest  
814 Service, Rocky Mountain Research Station, Fort Collins, CO, 428.

815 CARRETIER, S., TOLORZA, V., RODRIGUEZ, M.P., PEPIN, E., AGUILAR, G., REGARD, V., MARTINOD, J., RIQUELME, R.,  
816 BONNET, S., BRICHAU, S., HERAIL, G., PINTO, L., FARIAS, M., CHARRIER, R. & GUYOT, J.L. (2015) Erosion  
817 in the Chilean Andes between 27 Degrees S and 39 Degrees S: Tectonic, Climatic and  
818 Geomorphic Control. *Geodynamic Processes in the Andes of Central Chile and Argentina*, **399**,  
819 401-418.

820 CHURCH, M. & KELLERHALS, R. (1978) Statistics of Grain-Size Variation Along a Gravel River. *Canadian  
821 Journal of Earth Sciences*, **15**, 1151-1160.

822 CONSTANTINE, C.R., MOUNT, M.F. & FLORSHEIM, J.L. (2003) The Effects of Longitudinal Differences in Gravel  
823 Mobility on the Downstream Fining Pattern in the Cosumnes River, California. *Journal of  
824 Geology*, **111**, 233-241.

825 COVAULT, J.A., CRADDOCK, W.H., ROMANS, B.W., FILDANI, A. & GOSAI, M. (2013) Spatial and Temporal  
826 Variations in Landscape Evolution: Historic and Longer-Term Sediment Flux through Global  
827 Catchments. *Journal of Geology*, **121**, 35-56.

828 D'ARCY, M., WHITTAKER, A.C. & RODA-BOLUDA, D.C. (2017) Measuring Alluvial Fan Sensitivity to Past  
829 Climate Changes Using a Self-Similarity Approach to Grain-Size Fining, Death Valley, California.  
830 *Sedimentology* **64**, 388-424 doi:10.1111/sed.12308

831 DINGLE, E.H., SINCLAIR, H.D., ATTAL, M., MILODOWSKI, D.T. & SINGH, V. (2016) Subsidence Control on River  
832 Morphology and Grain Size in the Ganga Plain. *American Journal of Science*, **316**, 778-812.

833 DULLER, R.A., WHITTAKER, A.C., FEDELE, J.J., WHITCHURCH, A.L., SPRINGETT, J., SMITHELLS, R., FORDYCE, S. &  
834 ALLEN, P.A. (2010) From Grain Size to Tectonics. *Journal of Geophysical Research-Earth Surface*,  
835 **115**.

836 FEDELE, J.J. & PAOLA, C. (2007) Similarity Solutions for Fluvial Sediment Fining by Selective Deposition.  
837 *Journal of Geophysical Research-Earth Surface*, **112**.

838 FERGUSON, R.I., CUDDEN, J.R., HOEY, T.B. & RICE, S.P. (2006) River System Discontinuities Due to Lateral  
839 Inputs Generic Styles and Controls. *Earth Surface Processes and Landforms* **31**, 1149-1166  
840 doi:10.1002/esp.1309

841 FERNÁNDEZ-SEVESO, F. (1993) Sismoestratigrafía De La Cuenca Iglesia: Informe De Actividades En La  
842 Universidad De Cornell. **Informe Interne 10.408**, 20.

843 FORZONI, A., STORMS, J.E.A., WHITTAKER, A.C. & DE JAGER, G. (2014) Delayed Delivery from the Sediment  
844 Factory: Modeling the Impact of Catchment Response Time to Tectonics on Sediment Flux and  
845 Fluvio-Deltaic Stratigraphy. *Earth Surface Processes and Landforms*, **39**, 689-704.

846 FOSTER, M.A., ANDERSON, R.S., GRAY, H.J. & MAHAN, S.A. (2017) Dating of River Terraces Along Lefthand  
847 Creek, Western High Plains, Colorado, Reveals Punctuated Incision. *Geomorphology*, **295**, 176-  
848 190.

849 GOMEZ, B., ROSSER, B.J., PEACOCK, D.H., HICKS, D.M. & PALMER, J.A. (2001) Downstream Fining in a Rapidly  
850 Aggrading Gravel Bed River. *Water Resources Research*, **37**, 1813-1823.

851 HARRIES, R.M., KIRSTEIN, L., WHITTAKER, A., ATTAL, M., PERALTA, S. & BROOKE, S. (2018) Evidence for Self-  
852 Similar Bedload Transport on Andean Alluvial Fans, Iglesia Basin, South Central Argentina  
853 *Journal Of Geophysical Research: Earth Surface*, **123**, 2292-2315.

854 HELLER, P.L. & PAOLA, C. (1992) The Large-Scale Dynamics of Grain-Size Variation in Alluvial Basins, 2  
855 Application to Syntectonic Conglomerate, Basin Research Volume 4, Issue 2. *Basin Research*  
856 **4**, 91-102

857 HIRANO, M. (1971) River Bed Degradation with Armouring. *Proceedings of the Japanese Society of Civil*  
858 *Engineering*, **195**, 55-65.

859 HOEY, T.B. & FERGUSON, R.I. (1997) Controls of Strength and Rate of Downstream Fining above a River  
860 Base Level Water Resources Research Volume 33, Issue 11. *Water Resources Research* **33**,  
861 2601-2608

862 HOEY, T.B. & BLUCK, B.J. (1999) Identifying the Controls over Downstream Fining of River Gravels.  
863 *Journal of Sedimentary Research*, **69**, 40-50.

864 HOVIUS, N. & LEEDER, M. (1998) Clastic Sediment Supply to Basins. *Basin Research*, **10**, 1-5.

865 HUMPHREY, N.F. & HELLER, P.L. (1995) Natural Oscillations in Coupled Geomorphic Systems - an  
866 Alternative Origin for Cyclic Sedimentation. *Geology*, **23**, 499-502.

867 JEROLMACK, D.J. & PAOLA, C. (2010) Shredding of Environmental Signals by Sediment Transport.  
868 *Geophysical Research Letters*, **37**.

869 JORDAN, T., FERNANDEZ, A., FERNANDEZ-SEVESO, F., RÉ, G. & MILANA, J.P. (1997) Relaciones Entre Las  
870 Historias Evolutivas De Las Cuencas De Iglesia Y Bermejo, Prov. De San Juan, Argentina. *Actas*  
871 *de las segundas jornadas sobre geologia de Precordillera*, 142-147.

872 KASS, R.E. & RAFTERY, A.E. (1995) Bayes Factors. *Journal of the American Statistical Association*, **90**, 773-  
873 795.

874 KELLERHALS, R. & BRAY, D.I. (1971) Improved Method for Size Distribution of Stream Bed Gravel. *Water*  
875 *Resources Research*, **7**, 1045.

876 KNIGHTON, A.D. (1980) Longitudinal Changes in Size and Sorting of Stream-Bed Material in 4 English  
877 Rivers. *Geological Society of America Bulletin*, **91**, 55-62.

878 LAMB, M.P., DIETRICH, W.E. & VENDITTI, J.G. (2008) Is the Critical Shields Stress for Incipient Sediment  
879 Motion Dependent on Channel-Bed Slope? *Journal of Geophysical Research-Earth Surface*,  
880 **113**.

881 LEE, M. & WAGENMAKERS, E.J. (2014) *Bayesian Cognitive Modeling: A Practical Course*. Cambridge  
882 University Press.

883 MALATESTA, L.C., AVOUAC, J.-P., BROWN, N.D., BREITENBACH, S.F.M., PAN, J., CHEVALIER, M.-L., RHODES, E.,  
884 SAINT-CARLIER, D., ZHANG, W., CHARREAU, J., LAVÉ, J. & BLARD, P.-H. (2018) Lag and Mixing During  
885 Sediment Transfer across the Tian Shan Piedmont Caused by Climate-Driven  
886 Aggradation? Incision Cycles Basin Research Early View. *Basin Research*, n/a

887 MALATESTA, L.C., PRANCEVIC, J.P. & AVOUAC, J.-P. (2017) Autogenic Entrenchment Patterns and Terraces  
888 Due to Coupling with Lateral Erosion in Incising Alluvial Channels. *Journal Of Geophysical*  
889 *Research: Earth Surface*, **122**, 335-355.

890 MASON, C.C. & ROMANS, B.W. (2018) Climate-Driven Unsteady Denudation and Sediment Flux in a High-  
891 Relief Unglaciaded Catchment-Fan Using 26al and 10be: Panamint Valley, California *Earth and*  
892 *Planetary Science Letters*.

893 MCPHILLIPS, D., BIERMAN, P.R., CROCKER, T. & ROOD, D.H. (2013) Landscape Response to Pleistocene-  
894 Holocene Precipitation Change in the Western Cordillera, Peru: Be-10 Concentrations in  
895 Modern Sediments and Terrace Fills. *Journal of Geophysical Research-Earth Surface*, **118**,  
896 2488-2499.

897 MEYER-PETER, E. & MULLER, R. (1948) Formulas for Bed-Load Transport. *Proceedings of the 2nd IAHR*  
898 *Meeting, Int. Assoc. of Hydraulic. Eng. and Res. Madrid*, 39-64.

899 MICHAEL, N.A., WHITTAKER, A.C. & ALLEN, P.A. (2013) The Functioning of Sediment Routing Systems Using  
900 a Mass Balance Approach: Example from the Eocene of the Southern Pyrenees. *Journal of*  
901 *Geology*, **121**, 581-606.

902 MUELLER, E.R., PITLICK, J. & NELSON, J.M. (2005) Variation in the Reference Shields Stress for Bed Load  
903 Transport in Gravel-Bed Streams and Rivers. *Water Resources Research*, **41**.

904 NICHOLS, K.K., BIERMAN, P.R., CAFFEE, M., FINKEL, R. & LARSEN, J. (2005) Cosmogenically Enabled Sediment  
905 Budgeting. *Geology*, **33**, 133-136.

906 NORTH, F.K. (1985) Exploration Seismology. In: *Petroleum Geology* (Ed. by, 418. Allen and Unwin Inc,  
907 Winchester, USA.

908 PAOLA, C., PARKER, G., SEAL, R., SINHA, S.K., SOUTHARD, J.B. & WILCOCK, P.R. (1992) Downstream Fining by  
909 Selective Deposition in a Laboratory Flume. *Science*, **258**, 1757-1760.

910 PAOLA, C. & SEAL, R. (1995) Grain-Size Patchiness as a Cause of Selective Deposition and Downstream  
911 Fining. *Water Resources Research*, **31**, 1395-1407.

912 PAOLA, C. & MARTIN, J.M. (2012) Mass-Balance Effects in Depositional Systems. *Journal of Sedimentary  
913 Research*, **82**, 435-450.

914 PARKER, G. (1978) Self-Formed Straight Rivers with Equilibrium Banks and Mobile Bed .2. Gravel River.  
915 *Journal of Fluid Mechanics*, **89**.

916 PARKER, G. (1991a) Selective Sorting and Abrasion of River Gravel .2. Applications. *Journal of Hydraulic  
917 Engineering-Asce*, **117**, 150-171.

918 PARKER, G. (1991b) Selective Sorting and Abrasion of River Gravel .2. Applications. *Journal of Hydraulic  
919 Engineering*, **117**, 150-171.

920 PARSONS, A.J., MICHAEL, N.A., WHITTAKER, A.C., DULLER, R.A. & ALLEN, P.A. (2012) Grain-Size Trends Reveal  
921 the Late Orogenic Tectonic and Erosional History of the South-Central Pyrenees, Spain. *Journal  
922 of the Geological Society*, **169**, 111-114.

923 PELLETIER, J.D., MURRAY, A.B., PIERCE, J.L., BIERMAN, P.R., BRESHEARS, D.D., CROSBY, B.T., ELLIS, M., FOUFOULA-  
924 GEORGIU, E., HEIMSATH, A.M., HOUSER, C., LANCASTER, N., MARANI, M., MERRITTS, D.J., MOORE, L.J.,  
925 PEDERSON, J.L., POULOS, M.J., RITTENOUR, T.M., ROWLAND, J.C., RUGGIERO, P., WARD, D.J., WICKERT,  
926 A.D. & YAGER, E.M. (2015) Forecasting the Response of Earth's Surface to Future Climatic and  
927 Land Use Changes: A Review of Methods and Research Needs. *Earths Future*, **3**, 220-251.

928 PERUCCA, L.P. & MARTOS, L.M. (2012) Geomorphology, Tectonism and Quaternary Landscape Evolution  
929 of the Central Andes of San Juan (30 Degrees S-69 Degrees W), Argentina. *Quaternary  
930 International*, **253**, 80-90.

931 PIZZUTO, J.E. (1995) Downstream Fining in a Network of Gravel-Bedded Rivers. *Water Resources  
932 Research*, **31**, 753-759.

933 RE, G.H., JORDAN, T.E. & KELLEY, S. (2003) Cronologia Y Paleogeografia Del Teriario De La Cuenca  
934 Intermontana De Iglesia Septentrional, Andes De San Juan, Argentina. *Revista de la Asociación  
935 Geológica Argentina*, **58**, 31-48.

936 RICE, S. & CHURCH, M. (1996) Sampling Surficial Fluvial Gravels: The Precision of Size Distribution  
937 Percentile Estimates. *Journal of Sedimentary Research*, **66**, 654-665.

938 RICE, S. (1998) Which Tributaries Disrupt Downstream Fining Along Gravel-Bed Rivers?  
939 *Geomorphology*, **22**, 39-56.

940 RICE, S. & CHURCH, M. (1998) Grain Size Along Two Gravel-Bed Rivers: Statistical Variation, Spatial  
941 Pattern and Sedimentary Links. *Earth Surface Processes and Landforms*, **23**, 345-363.

942 RICE, S. (1999) The Nature and Controls on Downstream Fining within Sedimentary Links. *Journal of  
943 Sedimentary Research*, **69**, 32-39.

944 ROBINSON, R.A.J. & SLINGERLAND, R.L. (1998) Grain-Size Trends, Basin Subsidence and Sediment Supply  
945 in the Campanian Castlegate Sandstone and Equivalent Conglomerates of Central Utah. *Basin  
946 Research*, **10**, 109-127.

947 RODA-BOLUDA, D.C. & WHITTAKER, A.C. (2018) Normal Fault Evolution and Coupled Landscape Response:  
948 Examples from the Southern Apennines, Italy. *Basin Research*, **30**, 186-209.

949 ROMANS, B.W., CASTELLTORT, S., COVAULT, J.A., FILDANI, A. & WALSH, J.P. (2016) Environmental Signal  
950 Propagation in Sedimentary Systems across Timescales. *Earth-Science Reviews*, **153**, 7-29.

951 RUSKIN, B.G. (2006) Sequence Stratigraphy and Paleopedology of Nonmarine Foreland Basins: Iglesia  
952 Basin, Argentina and Axhandle Basin, Utah, Cornell University, NY.

- 953 RUSKIN, B.G. & JORDAN, T.E. (2007) Climate Change across Continental Sequence Boundaries:  
954 Paleopedology and Lithofacies of Iglesia Basin, Northwestern Argentina. *Journal of*  
955 *Sedimentary Research*, **77**, 661-679.
- 956 SEAL, R., PAOLA, C., PARKER, G., SOUTHARD, J.B. & WILCOCK, P.R. (1997) Experiments on Downstream Fining  
957 of Gravel .1. Narrow-Channel Runs. *Journal of Hydraulic Engineering-Asce*, **123**, 874-884.
- 958 SHIELDS, A. (1936) Anwendung Der Aehnlichkeitsmechanik Und Der Turbulenzforschung Auf Die  
959 Geschiebebewegung. *Mltt. Preuss. Versuchsanst. Wasserbau Schiffbau*, **26**.
- 960 SIAME, L.L., BOURLES, D.L., SEBRIER, M., BELLIER, O., CASTANO, J.C., ARAUJO, M., PEREZ, M., RAISBECK, G.M. &  
961 YIOU, F. (1997) Cosmogenic Dating Ranging from 20 to 700 Ka of a Series of Alluvial Fan  
962 Surfaces Affected by the El Tigre Fault, Argentina. *Geology*, **25**, 975-978.
- 963 SINGER, M.B. (2008) Downstream Patterns of Bed Material Grain Size in a Large, Lowland Alluvial River  
964 Subject to Low Sediment Supply. *Water Resources Research*, **44**.
- 965 SNYDER, D.B. (1988) Foreland Crustal Geometries in the Andes of Argentina and the Zagros of Iran from  
966 Seismic Reflection and Gravity Data: Phd Thesis, Cornell University, Ithaca, NY.
- 967 SURIANO, J., LIMARINO, C.O., TEDESCO, A.M. & ALONSO, M.S. (2015) Sedimentation Model of Piggyback  
968 Basins: Cenozoic Examples of San Juan Precordillera, Argentina. *Geodynamic Processes in the*  
969 *Andes of Central Chile and Argentina*, **399**, 221-244.
- 970 SYVITSKI, J.P.M. & MILLIMAN, J.D. (2007) Geology, Geography, and Humans Battle for Dominance over  
971 the Delivery of Fluvial Sediment to the Coastal Ocean. *Journal of Geology*, **115**, 1-19.
- 972 VAL, P., HOKE, G.D., FOSDICK, J.C. & WITTMANN, H. (2016) Reconciling Tectonic Shortening, Sedimentation  
973 and Spatial Patterns of Erosion from Be-10 Paleo-Erosion Rates in the Argentine Precordillera.  
974 *Earth and Planetary Science Letters*, **450**, 173-185.
- 975 VON BLANCKENBURG, F. (2006) The Control Mechanisms of Erosion and Weathering at Basin Scale from  
976 Cosmogenic Nuclides in River Sediment (Vol 237, Pg 462, 2005). *Earth and Planetary Science*  
977 *Letters*, **242**, 223-239.
- 978 WATERS, J.V., JONES, S.J. & ARMSTRONG, H.A. (2010) Climatic Controls on Late Pleistocene Alluvial Fans,  
979 Cyprus. *Geomorphology*, **115**, 228-251.
- 980 WHITTAKER, A.C., ATTAL, M. & ALLENN, P.A. (2010) Characterising the Origin, Nature and Fate of Sediment  
981 Exported from Catchments Perturbed by Active Tectonics. *Basin Research*, **22**, 809-828.
- 982 WHITTAKER, A.C., DULLER, R.A., SPRINGETT, J., SMITHELLS, R.A., WHITCHURCH, A.L. & ALLEN, P.A. (2011)  
983 Decoding Downstream Trends in Stratigraphic Grain Size as a Function of Tectonic Subsidence  
984 and Sediment Supply. *Geological Society of America Bulletin*, **123**, 1363-1382.
- 985 WILCOCK, P.R. & KENWORTHY, S.T. (2002) A Two-Fraction Model for the Transport of Sand/Gravel  
986 Mixtures Water Resources Research Volume 38, Issue 10. *Water Resources Research* **38**, 12-  
987 11-12-12
- 988 WITTMANN, H., VON BLANCKENBURG, F., MAURICE, L., GUYOT, J.L., FILIZOLA, N. & KUBIK, P.W. (2011) Sediment  
989 Production and Delivery in the Amazon River Basin Quantified by in Situ-Produced Cosmogenic  
990 Nuclides and Recent River Loads. *Geological Society of America Bulletin*, **123**, 934-950.

991

992

993 Appendix

994

995 *A1. Self-similar grain size distributions and relative mobility function J*

996

997 Self-similarity among the size distributions of riverbed gravel refers to the scale-invariant shape of  
998 their distribution. If the gravel deposits are self-similar, their  $C_V$  should to be relatively constant for  
999 any downstream distance, where distance is normalized by the length,  $L$ , of the depositional system,  
1000  $x^* = X/L$ . In this case, Fedele and Paola (2007) show a similarity variable,  $\xi$ , can be derived using:

1001 
$$\xi = \frac{D - \bar{D}(x^*)}{\sigma(x^*)} \quad \text{Equation A1}$$

1002 where  $D$  is the size of each individual grain in a distribution. This self-similar behaviour is predictable  
1003 through a simplification of the Exner sediment mass balance equation for when the Shields parameter,  
1004 i.e. the non-dimensionalized critical shear stress required for particle entrainment, is cross-sectionally  
1005 averaged. In this case, sediment transport and deposition, typically described by Hirano's three layer  
1006 sediment sorting model (Hirano, 1971), can be expressed as a simple, probabilistic partitioning ratio  
1007 between the size fraction of clasts in transport,  $p_i$ , and the size fraction on the bed surface,  $F_{.i}$ .

1008 
$$J_i = p_i / F_{.i} \quad \text{Equation A2}$$

1009 where the mobility function,  $J_i$ , describes the relative mobility of clast sizes deposited locally (Fedele  
1010 & Paola, 2007; Duller *et al.*, 2010). Assuming both the bed surface size distributions and the form of  
1011 the relative mobility function,  $J$ , can be collapsed into the same similarity solution, the bed surface  
1012 size distribution can be used to reconstruct  $J$ .

1013 Fedele and Paola (2007) derive a function for  $J$  using a semi-empirical, hydraulically based fining  
1014 model, ACRONYM, calibrated against field and experimental data (Parker, 1991b) and based on their  
1015 transformation of the measured grain size distributions into self-similar  $\xi$  distributions. They  
1016 parameterize the relative mobility function  $J$  as:

1017 
$$J_i = a_g e^{-b_g \xi} + c_g \quad \text{Equation A3}$$

1018 where  $a_g$ ,  $b_g$  and  $c_g$  are constants that characterise the incipient motion of gravel. Sediment  
1019 entrainment is considered dependent solely on particle size; therefore,  $a_g$  scales with the mobility of  
1020 all clast sizes,  $b_g$  describes the rate at which clasts of increasing size become less mobile than smaller  
1021 clasts, and  $c_g$  relates to the minimum probability of entraining a clast of any size. The shape and  
1022 structure of the relative mobility function  $J$  is expected to depend on the nature of the transport

1023 regime; the formulation above is for sediments coarser than sand (Whittaker *et al.*, 2011; D'Arcy *et*  
1024 *al.*, 2017), for which bed load transport is likely to be the dominant mode.

## 1025 *A2. Impact of abrasion on downstream grain size fining in the Iglesia basin*

1026

1027 The breakdown of clasts during sediment transport is dependent on the resistance of clasts to abrasion  
1028 and the distance over which the clasts have been transported (Attal & Lavé, 2009). Abrasion should  
1029 contribute to downstream fining on alluvial fan, and we assess its relative contribution to the fining  
1030 trends by observing how the proportions of clast lithologies in our samples change downstream.

1031 We sampled the lithology and size of 200 clasts at each sample location using a Wolman point count  
1032 technique for clast selection, i.e., clasts were selected randomly from a predefined area  $\sim 2\text{m}^2$ . The b-  
1033 axis of each clast was measured and its lithology categorised as Intrusive, Extrusive, Sedimentary,  
1034 Metamorphic or Quartzite. In figure A1, the proportions of the different lithologies present at each  
1035 site are plotted against their distance downstream, from fan apex to toe.

1036 Intrusive and extrusive rocks are expected to abrade at a low rate, typically less than 1 % mass loss /  
1037 km, equivalent to a downstream fining rate of 0.3 % / km (Attal *et al.*, 2006; Attal & Lavé, 2009).  
1038 However, the abrasion rate of sedimentary rocks, which make up to half of the gravel on the fans, is  
1039 more difficult to constrain. If sedimentary rocks were abraded faster than the other rocks, then we  
1040 would expect a systematic downstream decrease in the relative proportion of sedimentary gravel with  
1041 respect to the other rock types. We observe no systematic change in the relative proportion of  
1042 lithologies across fans 2 and 3, suggesting no preferential abrasion of any particular lithology on these  
1043 fans (figure A1). We can therefore assume that all gravel is as resistant, with an abrasion rate unlikely  
1044 to exceed 1 % mass loss / km, and therefore a minimal contribution to the observed downstream  
1045 fining at rates of 6.7 and 5.9 % / km on fans 2 and 3, respectively.

1046 On fan 1 however, we note that the contribution of gravel from sedimentary rocks gradually decreases  
1047 from  $\sim 50$  % of all gravel at the apex of the fan to  $\sim 30$  % at a distance of nearly 40 km downstream,  
1048 while the relative proportion of extrusive gravel and quartzite increases (figure A1). This suggests that  
1049 the gravel made of sedimentary rocks is abraded faster than the others, and that abrasion may  
1050 therefore contribute to the observed downstream fining on the fan. To assess the magnitude of the  
1051 phenomena, we run a very simple model of gravel abrasion that predicts the evolution of a mixture  
1052 made of hard and soft gravel abrading at two different rates (Supplementary Information). We find  
1053 that if the hard rocks are abrading at a conservative rate of 1 % mass loss / km, then the soft gravel  
1054 needs to abrade at a rate of 3.1 % / km to have its contribution reduced from 50 to 30 % over a distance



1055 of 40 km. The equivalent mass loss rate for the mixture is 1.9 % / km, equivalent to a fining rate of 0.6  
1056 % / km (Supplementary Information). Because the fining rate observed on fan 1 is 1.8 % / km, we  
1057 conclude that abrasion may contribute up to 30 % of the observed fining rate. We note that this is a  
1058 conservative estimate: we used a mass loss rate for the hard rock of 1 % / km but most of the change  
1059 in relative lithological proportions observed is driven by quartzite, which tends to abrade at a much  
1060 lower rate, typically 0.1-0.2 % / km.

### 1061 *A3. Varying basin subsidence*

1062

1063 In figure A2, alongside the measured grain size fining trends, we present modelled downstream grain  
1064 size fining trends for a range of other subsidence profiles that have no physical constraint other than  
1065 their wavelength, which is set by the width of the basin. Without prior constraint on the profile of  
1066 basin subsidence, the data can be fitted using the single source model with an exponential subsidence  
1067 profile typical of a normal-fault-bounded basin. This predicted profile is the inverse of the basin  
1068 structure that we measure. Fan 2 is fitted well by a subsidence profile with an exponent of  $0.05 \text{ m}/x^*$ ,  
1069 which yields a maximum subsidence rate of 1.7 m/10kyr. Fining profiles on fans 1 and 3 are less well  
1070 fitted by this profile of subsidence and this is due to the fact that relatively coarse gravel is still found  
1071 up to the toe of these fans; a characteristic that is difficult to resolve with a model solution that  
1072 assumes 100% of gravel sizes are exhausted at the maximum downstream length. This experiment  
1073 highlights the uncertainty in fitting self-similar grain size fining models to field data.

### 1074 *A4. Tributary Inputs*

1075

	Non-linear least squares regression	68% ( $\sigma$ ) confidence	95% ( $2\sigma$ ) confidence	RMSE	$p$ -value for $\alpha$	$\hat{l}_1$
Fan 1	$D_0 = 93 \text{ mm}$ $\alpha = -0.018/\text{km}$	$D_0 = 88 \text{ mm } \alpha = -0.022/\text{km}$ $D_0 = 99 \text{ mm } \alpha = -0.014/\text{km}$	$D_0 = 79 \text{ mm } \alpha = -0.028/\text{km}$ $D_0 = 107 \text{ mm } \alpha = -0.009/\text{km}$	12.07	0.006	7.29
Fan 2	$D_0 = 164 \text{ mm}$ $\alpha = -0.067/\text{km}$	$D_0 = 145 \text{ mm } \alpha = -0.081/\text{km}$ $D_0 = 182 \text{ mm } \alpha = -0.054/\text{km}$	$D_0 = 122 \text{ mm } \alpha = -0.099/\text{km}$ $D_0 = 205 \text{ mm } \alpha = -0.037/\text{km}$	23.02	0.019	8.35
Fan 3	$D_0 = 119 \text{ mm}$ $\alpha = -0.059/\text{km}$	$D_0 = 114 \text{ mm } \alpha = -0.061/\text{km}$ $D_0 = 123 \text{ mm } \alpha = -0.052/\text{km}$	$D_0 = 106 \text{ mm } \alpha = -0.069/\text{km}$ $D_0 = 130 \text{ mm } \alpha = -0.045/\text{km}$	7.169	0.001	6.02

1076

1077 *Table 1: Empirical model fit to data. The exponential relation that attains a log-likelihood function,  $\hat{l}_1$ , with the lowest residual sum of squares is reported as the intercept grain*  
1078 *size,  $D_0$ , and the downstream fining exponent  $\alpha$ , for each respective fan. We quote the Root Mean Square Error (RMSE) and the  $p$ -value for the fining exponent,  $\alpha$ . The table*  
1079 *includes the 68 and 95 % confidence intervals on this empirical best fit to the data.*

1080

1081

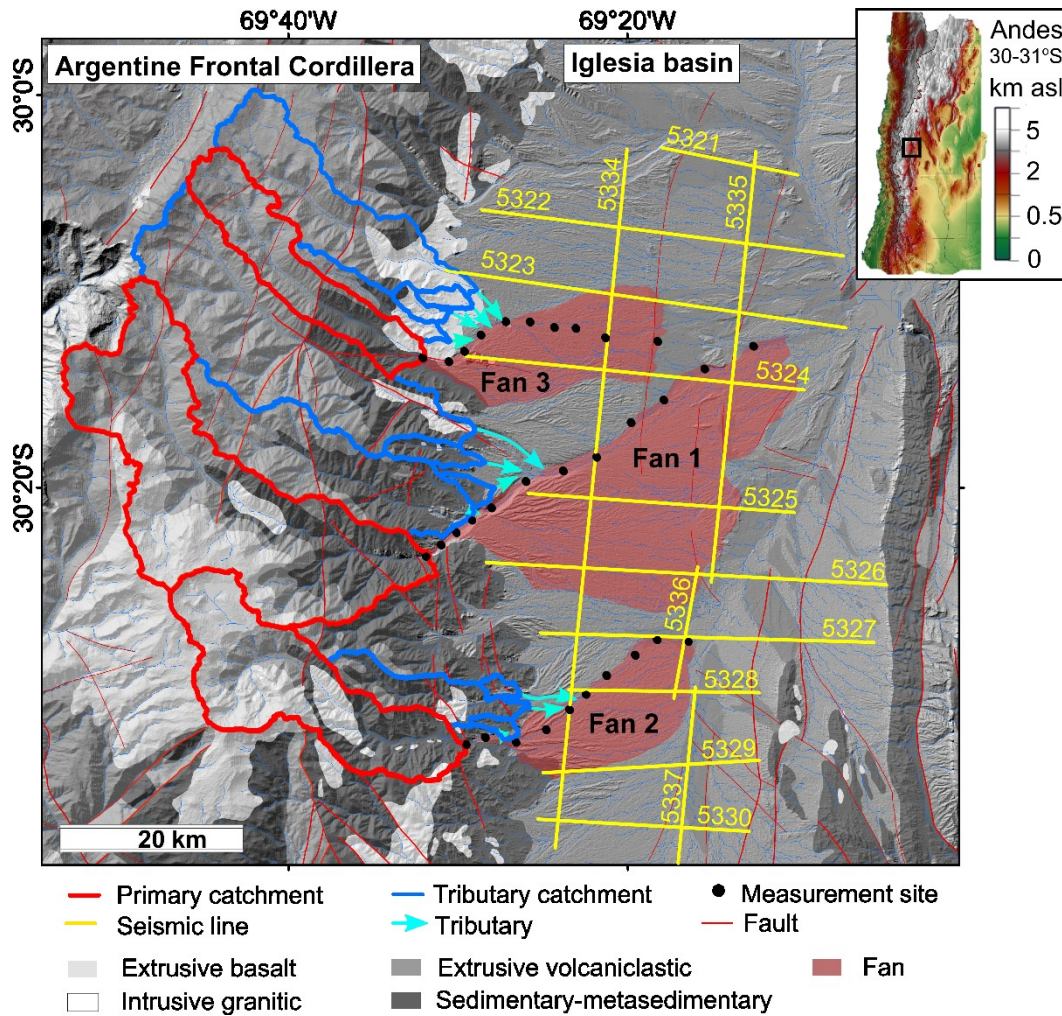
1082

	Fan 1		Fan 2		Fan 3	
	$x^*$	% $q_s$	$x^*$	% $q_s$	$x^*$	% $q_s$
Primary catchment	0	54	0	82	0	32
Tributary catchments	0.17	16	0.54	1	0.31	15
	0.33	1	0.58	17	0.38	16
	0.36	2			0.42	47
	0.38	27				1087

1088

1089 *Table A1: Percentage of the total sediment flux, %  $q_s$ , supplied by each catchment at the normalised downstream*  
 1090 *distance,  $x^*$ , along the trunk stream. Each catchment is delineated in figure 1. Sediment fluxes were estimated*  
 1091 *using the BQART sediment flux model after Syvitski and Milliman (2007) (Harries et al., 2018). Tributary*  
 1092 *confluences were mapped from satellite imagery.*

1093



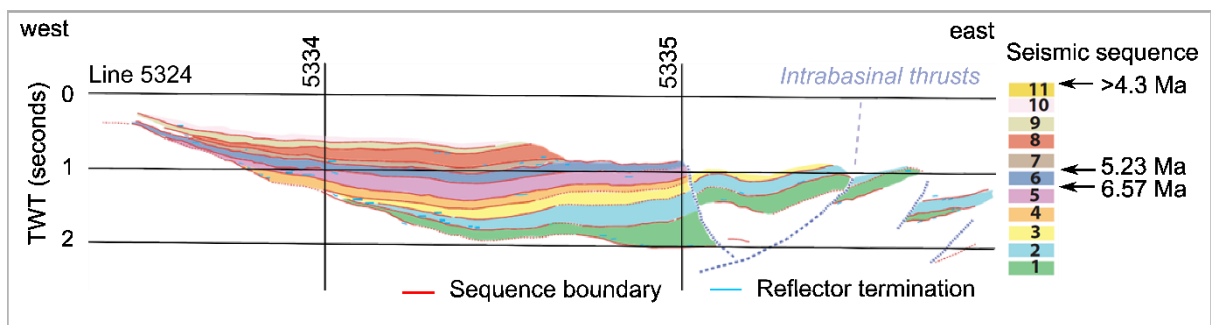
1094

1095

1096 *Figure 1: The Iglesia basin catchment-alluvial fans. Bedrock lithology and faults are taken from geological maps*  
 1097 *produced by the Argentine Servicio Geologico Minero (SEGEMAR). Seismic survey lines are taken from Ruskin*  
 1098 *(2006) and Beer (1990). There are ten west-east profiles ~25-35 km in length and four north-south tie lines,*  
 1099 *between 15 and 75 km in length. The top right inset is an ETOPO1 relief model, downloaded from the NCEI*  
 1100 *database (Amante & Eakins, 2009) which highlights the location of the Iglesia basin in the eastern foreland of*  
 1101 *the Andean mountain chain, 30-31°S. Photographs show tributaries and incised fan surfaces are important*  
 1102 *geomorphic features on these large alluvial piedmonts.*

1103

1104



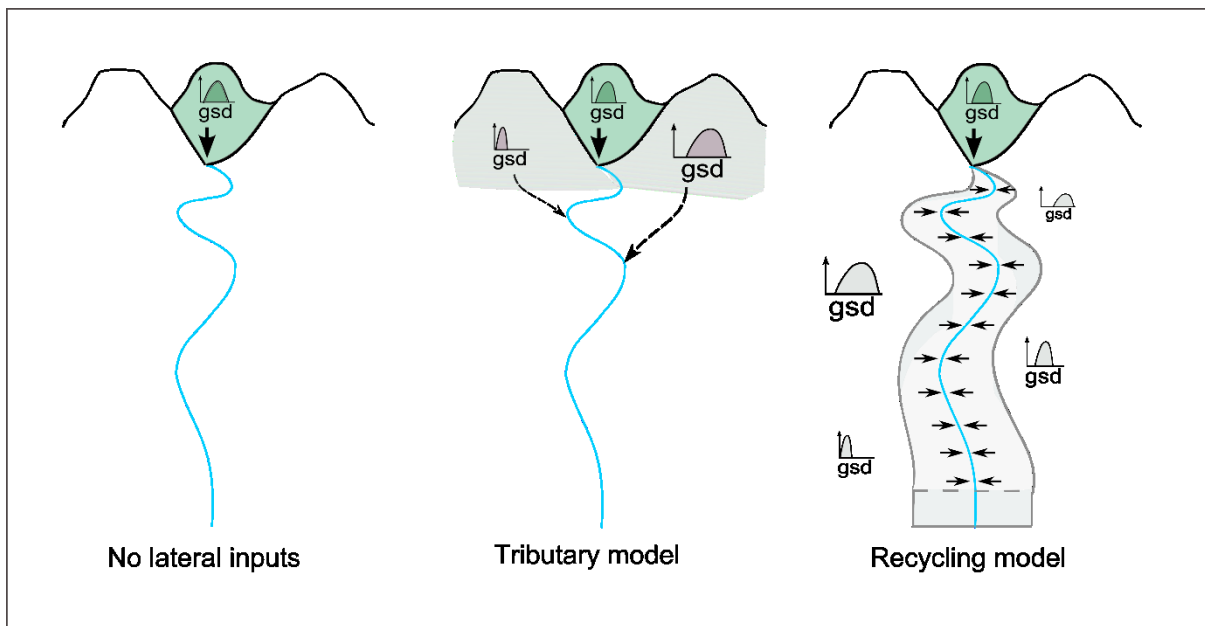
1105

1106 *Figure 2: Interpretation of seismic data collected close to the basin axis, along line 5324, adapted from Ruskin*  
1107 *(2006)*

1108

1109

1110



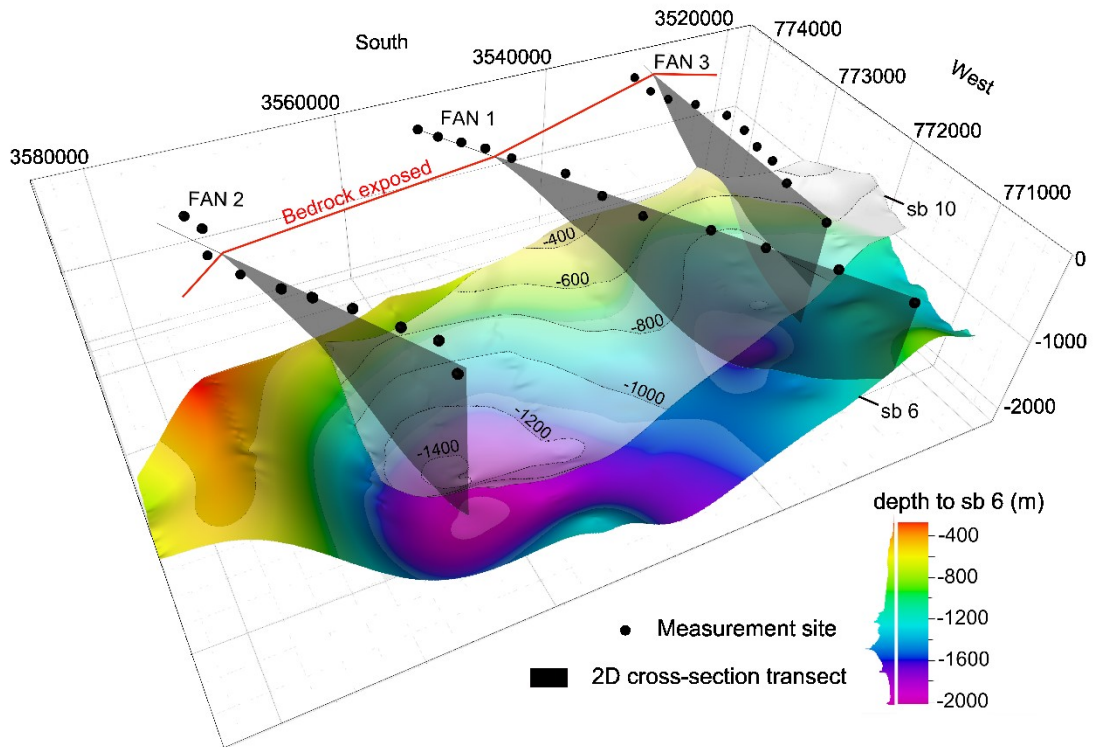
1111

1112 *Figure 3: Idealised end-member models for sediment sourcing on alluvial piedmonts. The no lateral inputs model,*  
1113 *or single input model, is typically used in sediment routing system modelling. The tributary model illustrates the*  
1114 *lateral incorporation of sediment from additional point sources with potentially very different grain size*  
1115 *distributions to the trunk stream (gsd). The recycling model captures the lateral incorporation of sediment by*  
1116 *older fan surface reworking. The sediment is supplied along the length of the depositional system and the grain*  
1117 *size distributions of recycled fan material are likely spatially variable. Within the self-similar model, the flux and*  
1118 *grain size of the sediment supplies are free parameters, though within each iteration we keep the gsd of all inputs*  
1119 *the same in order to reduce complexity.*

1120

1121

1122



1123

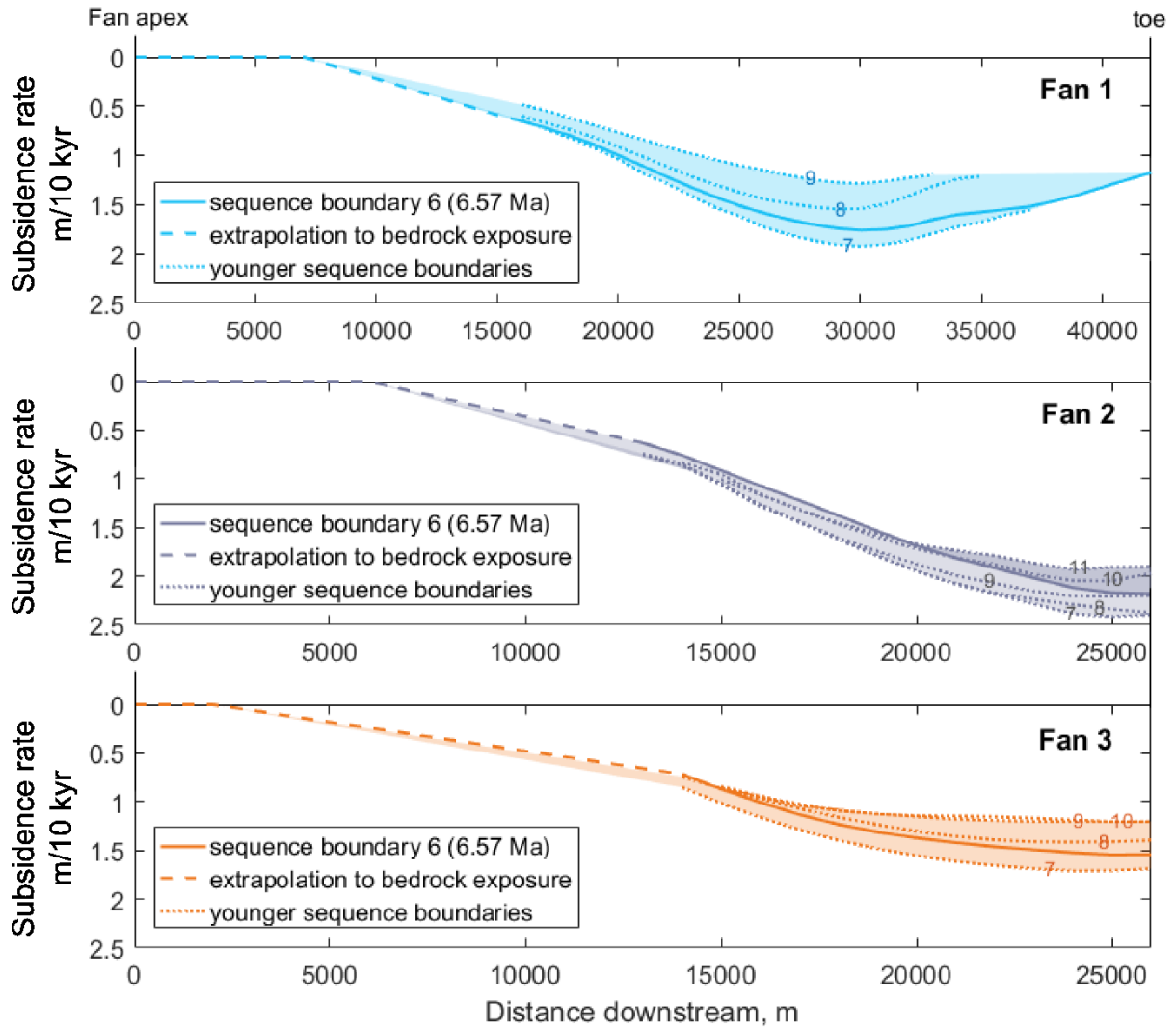
1124 *Figure 4: 3D model of the stratigraphy of the Iglesia basin. The isopachs of two sequence boundaries are plotted.*  
1125 *The oldest boundary, sb6, is the coloured surface where the isopach depth is given in the legend alongside its*  
1126 *hypometric depth distribution. The youngest boundary with good spatial coverage, sb10 is plotted in white and*  
1127 *has isopach depth contours. Black dots highlight the locations at the surface of the Earth where grain size*  
1128 *measurements were taken for each fan and the red line delineates where bedrock is exposed. Depth slices outline*  
1129 *the transect along which 2D subsidence profiles were extracted for each fan.*

1130

1131

1132

1133

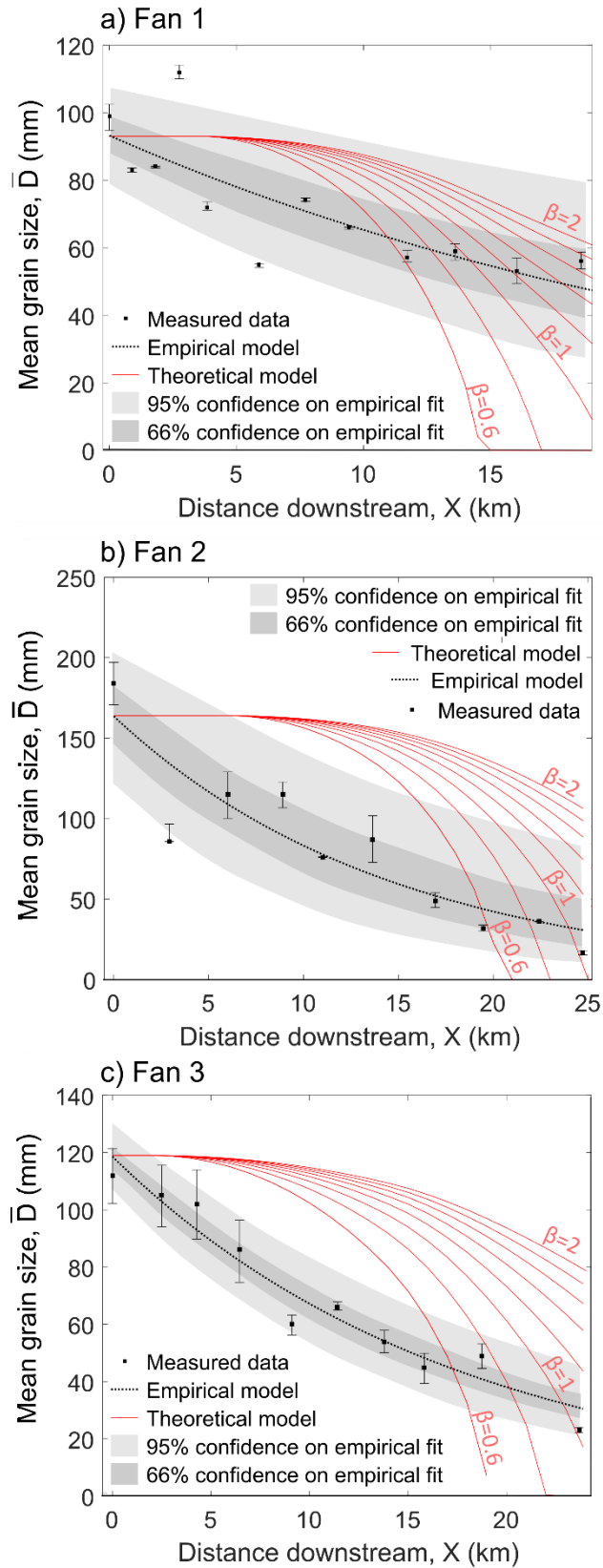


1134

1135 *Figure 5: Spatial distribution of differential subsidence along 2D transects highlighted in figure 4. Transects are*  
 1136 *taken from the fan apex to toe and are plotted as downstream distance from the fan apex. The sequence*  
 1137 *boundary cross-sections are numbered and correspond with respective isopach maps in appendix figure A1. For*  
 1138 *fan 3, sb11 is not well imaged; similarly, for fan 1, sb 10 and 11 are only partially imaged and are therefore*  
 1139 *omitted from the analysis. The younger sequences are poorly imaged or discontinuous in the west of the basin,*  
 1140 *which results in an apparent overlapping of sb 10 and 11 for fan 2 and sb 9 and 10 for fan 3, where boundaries*  
 1141 *have been extrapolated toward the mountain front tracing the sb below. Sequence boundary 6 is used to*  
 1142 *constrain subsidence in the self-similar fining model as this is the most continuous sequence boundary mapped.*

1143

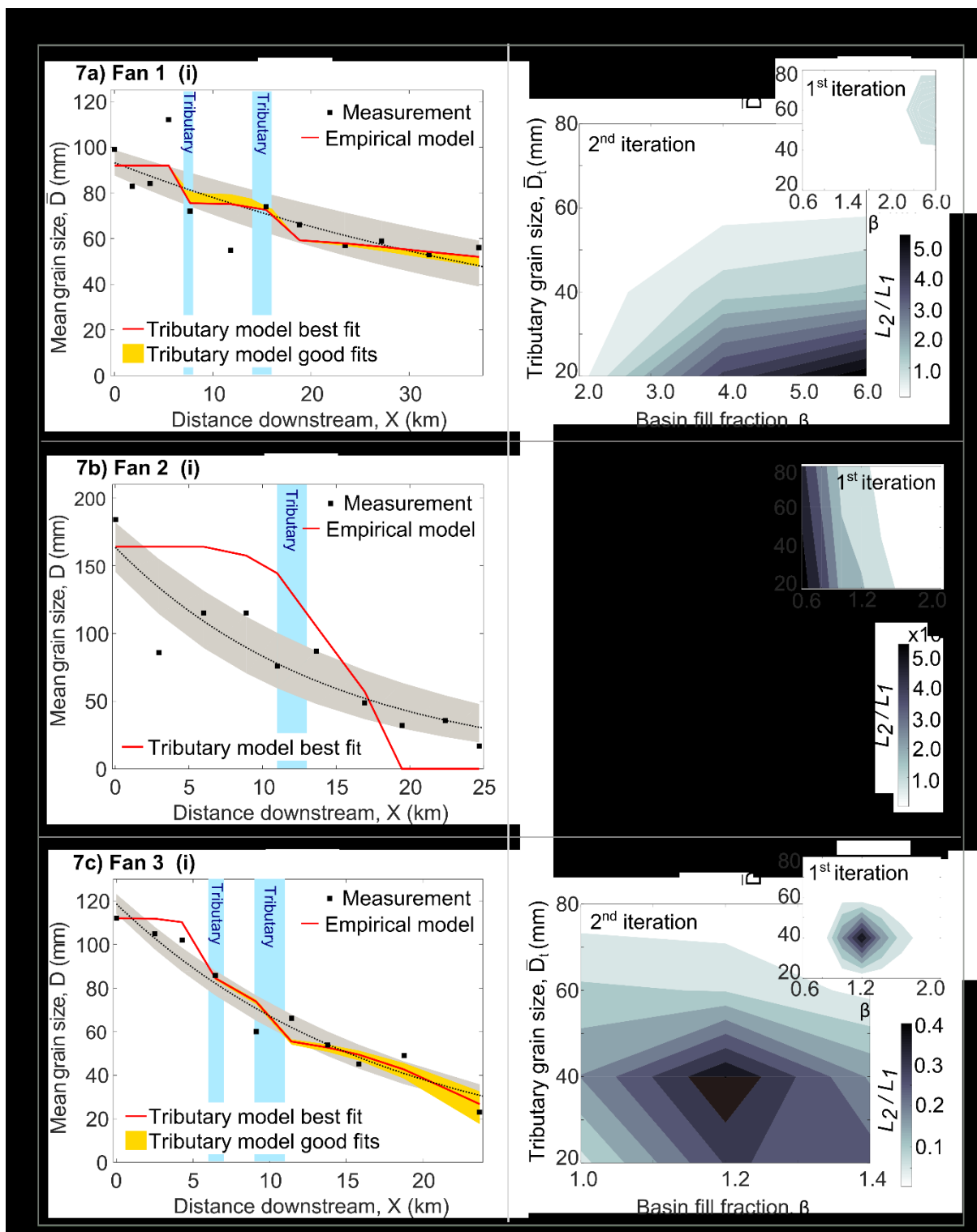




1144

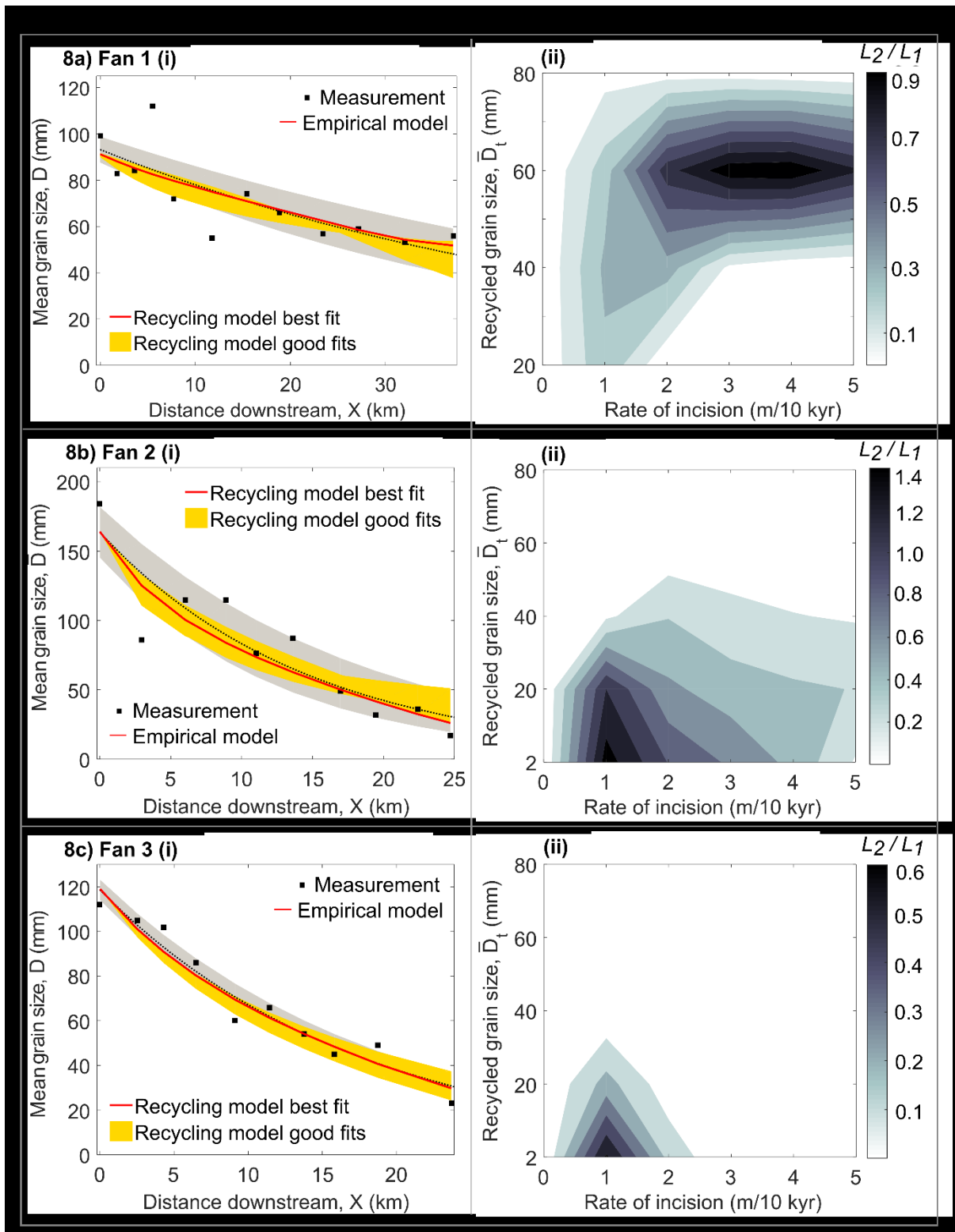
1145 *Figure 6: Single input model solutions for a range of basin fill fractions,  $\beta$ .*

1146



1148

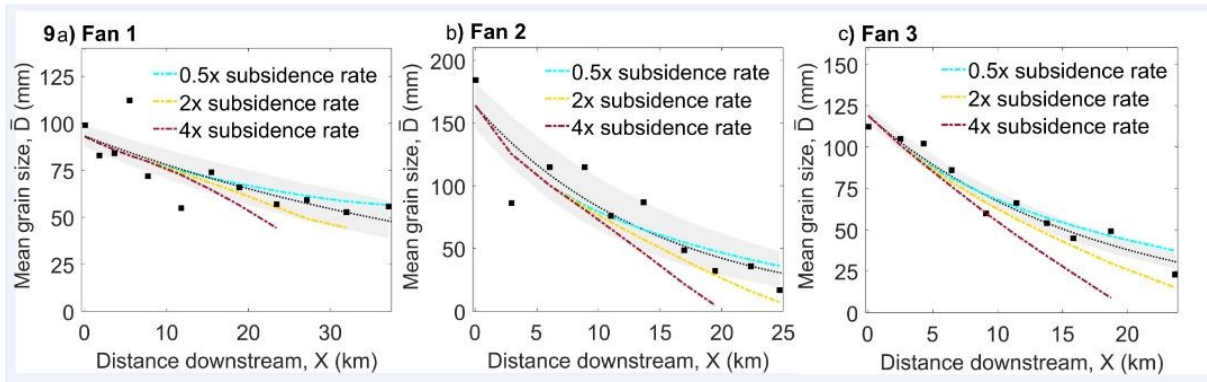
1149 *Figure 7: (i) Best fit and good fit tributary model solutions for grain size data on each fan. (ii) Isopachs of the*  
 1150 *likelihood ratio calculated for each model solution. For the first iteration, all tributary inputs have the same input*  
 1151 *grain size  $D_t$ . On the second iteration, the grain size of the lower fan tributaries is fixed at the best fit solution*  
 1152 *from the first iteration and the grain size of the upper fan tributaries is varied independently. A second iteration*  
 1153 *was not performed for fan 2 as the first iteration failed to find a good fit to the data.*



1155

1156 *Figure 8: (i) Best fit and good fit recycled model solutions for grain size data on each fan. (ii) Isopaches of the*  
 1157 *likelihood ratio calculated for each model solution.*

1158



1159

1160

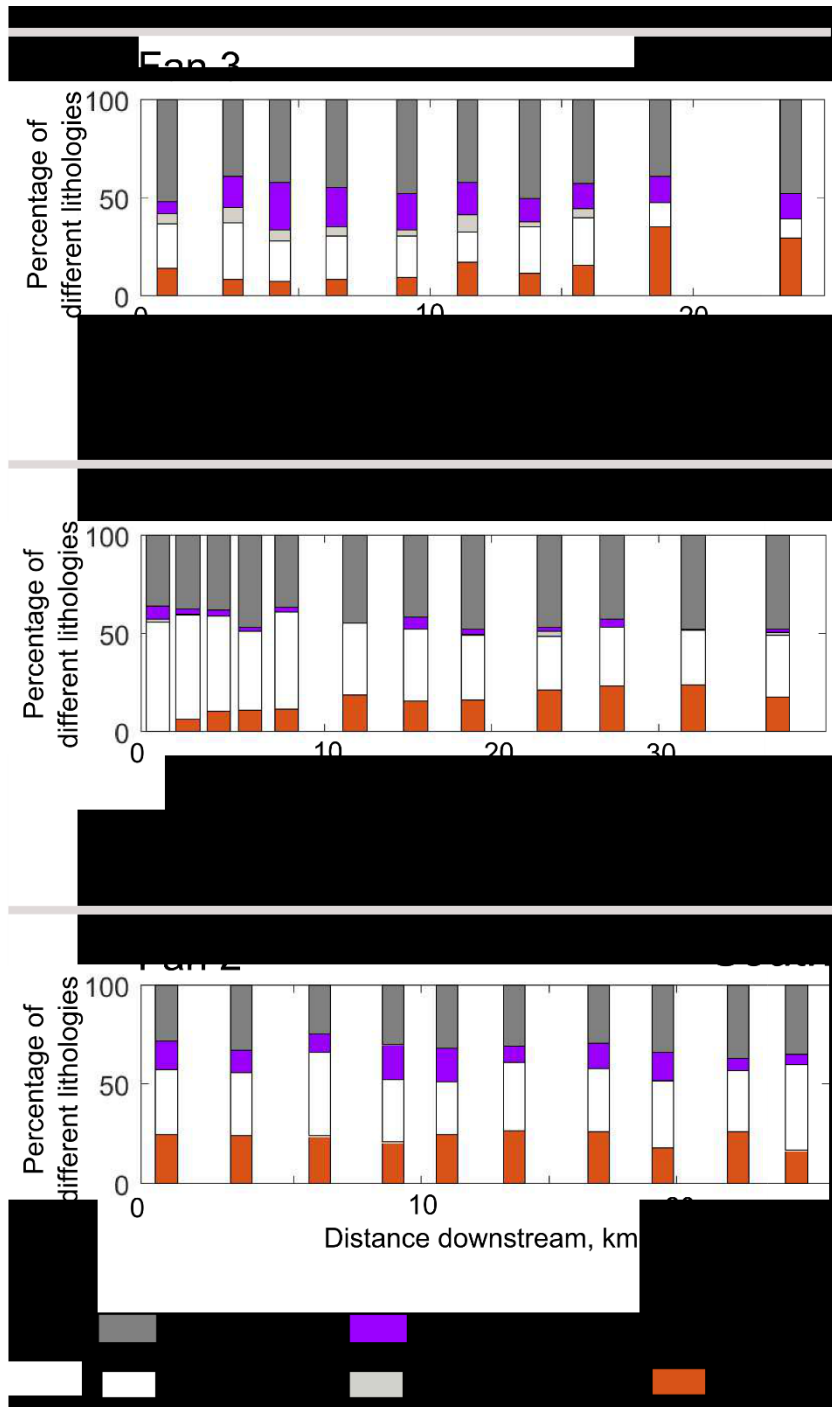
1161 *Summary figure 9: (a-c) Change in grain size fining profile of the best fit recycling model solution in response to*  
 1162 *a change in the rate of basin subsidence.*

1163

1164

1165

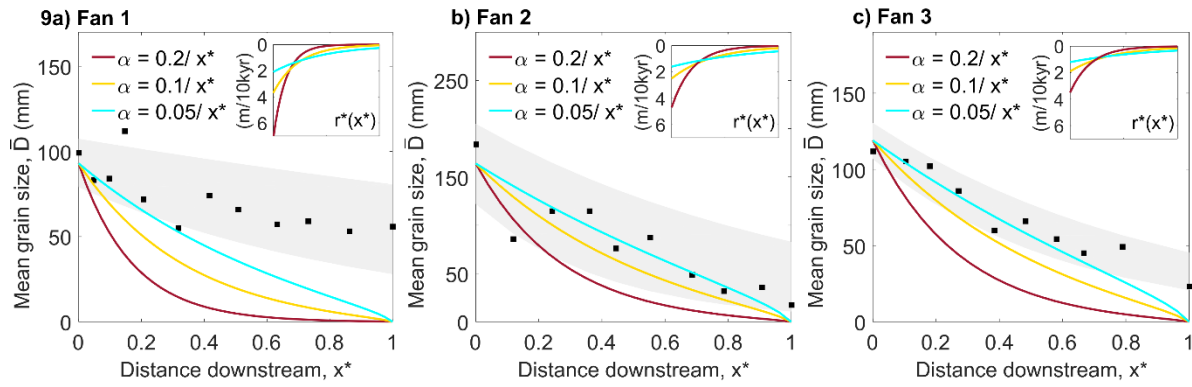
1166



1167

1168 *Figure A1: The proportions of different lithologies sampled at each site along the length of each fan.*

1169



1170

1171

1172 *Figure A2: Range of grain size fining model solutions attained for when the spatial distribution of tectonic*  
 1173 *subsidence,  $r^*(x^*)$ , is only constrained by the maximum width of the basin, by first order sediment flux*  
 1174 *estimations from the BQART model and an assumption that the basin is 100 % filled. The exponent of  $r^*(x^*)$  is*  
 1175 *varied between  $\alpha = 0.2$  and  $\alpha = 0.05$  to attain a fit to the data. The grey band is the 95% confidence interval for*  
 1176 *the fit of the empirical exponential to the measured data. The graphical insets plot the profiles of subsidence for*  
 1177 *when the exponent of  $r^*(x^*)$  is set to 0.2, 0.1 and 0.05, respectively.*



1179 *Figure A3: Isopach maps of sequence boundaries 6 to 11 constructed in Petrel™ using 2D seismic interpretations*  
1180 *of basin fill previously published in Ruskin (2006). Sequence boundaries (sb) 6 and 7 have previously established*  
1181 *age constraints (section 3.2) and sb 11 is given a minimum age of deposition of > 4.3 Ma. The ages of sb's 8-11*  
1182 *are estimated using rates of sediment accumulation at the average depth interval between sb 7 and sb 11, with*  
1183 *the spatial variation in accumulation rate given as a plus or minus error.*

1184